

1 **A global analysis of pollen-based reconstructions of land climate changes** 2 **during Dansgaard–Oeschger events**

3 Mengmeng Liu^{1,2,*}, Iain Colin Prentice¹, Sandy P. Harrison²

4 1: Georgina Mace Centre for the Living Planet, Department of Life Sciences, Imperial College
5 London, Silwood Park Campus, Buckhurst Road, Ascot SL5 7PY, UK

6 2: Department of Geography and Environmental Science, University of Reading, Reading,
7 RG6 6AB, UK

8 *** Corresponding author: Mengmeng Liu (m.liu18@imperial.ac.uk)**

9 Ms for: *Climate of the Past*

10 **Abstract**

11 Dansgaard–Oeschger (D–O) warming events are comparable in magnitude and rate to the
12 anticipated 21st century warming. As such, they provide a good target for evaluation of the
13 ability of state-of-the-art climate models to simulate rapid climate changes. Despite the wealth
14 of qualitative information about climate changes during the D–O events, there has been no
15 attempt to date to make quantitative reconstructions globally. Here we use frequency-corrected
16 Tolerance-weighted Weighted Averaging Partial Least Squares regression (*fx*TWA-PLS) to
17 reconstruct mean temperature of the coldest month, mean temperature of the warmest month,
18 and a plant-available moisture index across multiple D–O events between 50 and 30 ka based
19 on available pollen records across the globe. The reconstruction of plant-available moisture is
20 corrected for the impact of changing atmospheric CO₂ concentrations on plant water use
21 efficiency. These reconstructions show that the largest warming occurred in northern
22 extratropics, especially Eurasia, while western North America and the southern extratropics
23 were characterised by cooling. The change in winter temperature was significantly larger than
24 the change in summer temperature in the northern extratropics and the tropics, indicating that
25 the D–O warming events were characterised by reduced seasonality, but there was no
26 significant difference between the summer and winter temperature changes in the southern
27 extratropics. The antiphasing between northern and southern extratropical changes, and the
28 west-east pattern of cooling and warming in North America were generally consistent across
29 the eight D–O events examined, although coherency is greatest during the strongest events.

30 There was no globally consistent pattern between changes in moisture and changes in
31 temperature. These reconstructions can be used to evaluate the spatial patterns of changes in
32 temperature and moisture in the transient simulations of the D-O events planned as part of the
33 Palaeoclimate Modelling Intercomparison Project.

34 1. Introduction

35 Dansgaard–Oeschger (D–O) events are characterised in Greenland by a transition from cold
36 Greenland Stadial (GS) to warmer Greenland Interstadial (GI) conditions (Dansgaard et al.,
37 1993). The surface air temperature in Greenland increased by 10–16° C during the warming
38 phases; these warming events occurred over an interval of between 50 and 200 years (Huber et
39 al., 2006; Kindler et al., 2014). Thus, the D-O events offer a parallel in terms of speed to
40 projected future warming, although both the baseline state and the mechanism inducing this
41 warming differ from anticipated 21st century climate changes. D-O events could therefore
42 provide an opportunity to determine how well climate models that are used for future
43 projections can simulate rapid climate changes (Malmierca-Vallet et al., 2023), particularly
44 regional patterns of warming (and cooling) that are regarded as a challenge for modelling
45 (Doblas-Reyes et al., 2021; Lee et al., 2021) and are highly important in assessing the
46 vulnerability of human societies to future climate changes (IPCC, 2022).

47 Although D-O events are found throughout the last glacial period, the largest number and the
48 most regular patterning occurred during Marine Isotope Stage 3 (MIS 3; 57 to 29 ka) when
49 there were 11 separate events (D-O 15 to D-O 5), while earlier stage such as MIS 4 (71 to 57
50 ka) only had 3 separate events (D-O 18 to 16) (Kindler et al., 2014). The typical duration of a
51 cycle as manifested in Greenland is *ca.* 1500 years and is characterised by an initial short slow
52 warming, followed by an abrupt large warming in matter of decades, followed by a long slow
53 cooling over centuries to millennia, with a terminal phase of fast cooling (e.g. D-O 8, D-O 12);
54 however, there are also cycles in which the warming and cooling phases took roughly the same
55 time (e.g. D-O 5, D-O 6, D-O 9) (Kindler et al., 2014). The magnitude of changes also differ,
56 with both strong events (e.g. D-O 8, D-O 12) and weak events (e.g. D-O 9) (Kindler et al.,
57 2014).

58 The D-O signals are not just in Greenland – they are registered globally (Adolphi et al., 2018;
59 Corrick et al., 2020; Harrison and Sanchez-Goñi, 2010; Sánchez-Goñi et al., 2017; Voelker,
60 2002) and are reflected in changes in both temperature and precipitation. Both oceanic and ice-
61 core records indicate that temperature changes are out-of-phase between the northern and
62 southern hemispheres, and the southern hemisphere response both in terms of warming and
63 cooling phases is generally less abrupt (Dima et al., 2018; Vettoretti and Peltier, 2015). There
64 is a comparative lack of information from the continents about the manifestation of D-O events.

65 Shifts in vegetation types between GI and GS states have been interpreted as primarily a
66 temperature signal in the extratropics and a moisture signal in the tropics (Harrison and
67 Sanchez-Goñi, 2010). Speleothem records provide a good time-control on the synchronicity of
68 climate changes globally with the D-O events registered in Greenland (Adolphi et al., 2018;
69 Corrick et al., 2020), but the driver of this signal can either be temperature or precipitation
70 depending on the region. There are quantitative climate reconstructions based on terrestrial
71 pollen records from La Grande Pile (Guiot et al., 1993), Lago Grande di Monticchio (Huntley
72 et al., 1999), Padul (Camuera et al., 2022), El Cañizar de Villarquemado (Camuera et al., 2022;
73 Wei et al., 2021) and Lake Ohrid (Sinopoli et al., 2019), marine cores in the western
74 Mediterranean and offshore from Portugal (Sánchez-Goñi et al., 2002), diatom assemblages at
75 Les Echets, France (Ampel et al., 2010), chironomids from Lake Bergsee in central Europe
76 (Lapellegerie et al., 2024), bacterial membrane lipid records from the Eifel region (Zander et
77 al., 2024), isotopic measurements of earthworm calcite from the Rhine Valley (Prud'homme
78 et al., 2022) and clumped isotope measurements on snails in Hungary (Újvári et al., 2021).
79 Aside from the lack of comparable quantitative estimates from outside Europe, differences in
80 the methodology employed and in the specific climate variables reconstructed in each of these
81 studies limits their usefulness for model evaluation. In particular, given that there is still
82 uncertainty as to whether the D-O cycles are characterised by changes in seasonality such that
83 warming events are primarily driven by changes in winter (Flückiger et al., 2008; Zander et al.,
84 2024; Zumaque et al., 2025), in the regional strength of the warming (Harrison and Sanchez-
85 Goñi, 2010) and how warming relates to changes in moisture (Wei et al., 2021), there is a need
86 for more systematic reconstruction of seasonal climate changes.

87 In the paper, we provide reconstructed changes in seasonal temperatures and plant-available
88 moisture during the intervals corresponding to D-O warming events in Greenland between 50
89 and 30 ka based on available pollen records globally, using a standard regression-based
90 approach, f_x -corrected Tolerance-weighted Weighted Averaging Partial Least Squares
91 (f_x TWA-PLS: Liu et al., 2020, 2023). We also correct the reconstructions of plant-available
92 moisture to take account of the impact of lower CO₂ on plant water-use efficiency following
93 Prentice et al. (2022a). We analyse the regional patterns to identify key targets for model
94 evaluation.

95 2. Methods

96 2.1. Data sources

97 2.1.1. Modern pollen dataset

98 Modern pollen data were obtained from version 3 of the SPECIAL Modern Pollen Dataset
99 (SMPDSv3) (Harrison et al., 2025a). This global dataset was constructed by amalgamating and
100 standardising records from public repositories (e.g. Neotoma, Pangaea), existing regional
101 databases (e.g. European Modern Pollen Database, African Pollen Database), individual
102 publications and records provided by the original authors. The records were carefully screened
103 to remove duplicates that were present in more than one source. The modern samples were
104 obtained from multiple types of record, including pollen traps, surface samples, moss polsters
105 and different types of sediment, including cores from lakes and peatbogs, and section through
106 e.g. fluvial or loess deposits. In cases where the record was radiometrically dated, the database
107 preserves all samples younger than 50 yr B.P. However, some samples were undated and are
108 therefore recorded as modern if a collection date was given or assumed modern if not.

109 The dataset contains 26704 samples from 18202 different locations, and was created after
110 removing taxa that are not climatically diagnostic (e.g. obligate aquatics, carnivorous species,
111 cultivated plants). The dataset provides several levels of taxonomic aggregation; here we use
112 the most aggregated level, where woody species were generally combined at genus level and
113 herbaceous species at sub-family or family level unless they were palynologically distinctive,
114 occupied distinctive ecological niches and were sufficiently geographically widespread. This
115 "amalgamated" dataset contains relative abundance information for 1367 taxa. These samples
116 were aggregated by location (which is longitude, latitude and elevation) in order to remove
117 duplicates. Counts for *Quercus*, *Quercus* (deciduous) and *Quercus* (evergreen) were combined
118 because of inconsistent differentiation of *Quercus* pollen in different regional records.
119 Deciduous and evergreen oaks occupy different areas of climate space, particularly in terms of
120 seasonal moisture; specifically, evergreen oaks are typically found in areas characterised by
121 winter rainfall such as the Mediterranean. Nevertheless, since there are other plant taxa that are
122 similarly diagnostic of such regimes, the amalgamation of *Quercus* (deciduous) and *Quercus*
123 (evergreen) should not have a major effect on the robustness of our climate reconstructions.
124 We have tested this assumption by making reconstructions based on all taxa except *Quercus*
125 (Supplementary Materials, section 4). Taxa that occurred in less than 10 samples in the training

126 dataset were not used to make reconstructions because it is unlikely that the available samples
127 provided a reasonable estimate of the climate space occupied by these rare taxa (Liu et al.,
128 2020). After the location aggregation and the taxa filter, the dataset contains information on
129 18202 samples with relative abundance information for 609 taxa (Figure 1a).

130 We focus on three climate variables: mean temperature of the coldest month (MTCO), mean
131 temperature of the warmest month (MTWA), and a plant-available moisture index (α_{plant})
132 defined as the estimated ratio of actual to equilibrium evapotranspiration. These three variables
133 reflect ecophysiological controls on plant distribution (Harrison, 2020; Woodward, 1987) that
134 have been shown to independently influence the distribution and abundance of plant species
135 (Boucher-Lalonde et al., 2012; Wang et al., 2013; Wei et al., 2020). α_{plant} is a transformation
136 of the commonly used moisture index MI (defined as the estimated ratio of annual precipitation
137 to annual potential evapotranspiration) that emphasizes differences at the dry end of the climate
138 range, which have a more pronounced effect on vegetation distribution than differences at the
139 wet end (Prentice et al., 2017). Thus, α_{plant} can be better reconstructed from the pollen records
140 than MI.

141 The climate values at each SMPDSv3 site were obtained using a geographically-weighted
142 regression (GWR) of climatological values of mean monthly temperature, precipitation, and
143 fractional sunshine hours from the Climatic Research Unit Time-Series version 4.04 (CRU
144 TS4.04; Harris et al., 2020) dataset averaged over the period 1961–1990, which corresponds
145 to the interval from which most of the pollen samples were derived. GWR was to correct for
146 elevation differences between the CRU grid cells and the pollen sites. MTCO and MTWA were
147 taken directly from the GWR. MI was calculated for each site using SPLASH v1.0 (Davis et
148 al., 2017) based on daily values of precipitation, temperature and sunshine hours obtained using
149 a mean-conserving interpolation of the monthly values of each. MI was then transformed to
150 α_{plant} using the parametric Fu-Zhang formulation of the Budyko relationship (Supplementary
151 Materials, section 2). The climate space occupied by SMPDSv3 (Figure S1) samples a
152 reasonable range of global climate space and therefore should provide robust reconstructions
153 of climate changes under glacial conditions.

154 We use a global modern dataset for calibration of the pollen-climate relationships. The use of
155 a global dataset, rather than region-specific training data, relies on the principle of phylogenetic
156 niche conservatism (Harvey and Pagel, 1991; Qian and Ricklefs, 2004; Wang et al., 2025),
157 which states that traits tend to remain constant over time and that the climatic niches of specific

158 genera are also conservative (Harrison et al., 2025c). The use of a global dataset for calibration
159 makes it possible to sample a large range of climates, and thus makes it more likely that the
160 reconstructions of glacial climates are realistic and not confined to the limited climate range
161 sampled in any one region in modern times (Turner et al., 2020).

162 **2.1.2. Fossil pollen dataset**

163 The Abrupt Climate Changes and Environmental Responses (ACER) database (Sánchez-Goñi
164 et al., 2017) was originally created to provide a source of pollen and charcoal data for Marine
165 Isotope Stage 3 (MIS 3), which includes 93 records with sufficient resolution and dating control
166 to detect sub-millennial scale variability. Much more records covering MIS 3 have become
167 available since the compilation of the ACER database, such as the synthetic pollen databases
168 available for Siberia (Cao et al., 2019, 2020) and China (Zhou et al., 2023) and the global
169 Legacy 2 dataset (Li et al., 2025), which can substantially cover the spatial gaps in the original
170 ACER database. We obtained these data from public sources or directly from the authors and
171 used them to create an update: ACER2 (Harrison et al., 2025b), which contains 233 additional
172 records covering some part or all of MIS 3 (note that the original ACER records are not
173 included in ACER2 due to licensing issue). The two datasets are combined in our analyses to
174 serve as the fossil pollen dataset (Supplementary Materials, section 3) to reconstruct the past
175 climates. We focus on the 279 records (253 terrestrial records and 26 marine records) between
176 50 and 30 ka (Figure 1b; Table 1). The fossil pollen data are taxonomically harmonised to be
177 consistent with the SMPDSv3.

178 **2.2. Climate reconstruction method**

179 We use f_x -corrected Tolerance-weighted Weighted Averaging Partial Least Squares (f_x TWA-
180 PLS: Liu et al., 2020, 2023) regression to derive the pollen-climate relationships in the modern
181 training dataset, and then apply these relationships to reconstruct past climates from the fossil
182 pollen records (Figure 2). f_x TWA-PLS reduces the tendency of regression methods to compress
183 reconstructions towards the centre of the sampled climate range by applying a sampling
184 frequency correction to reduce the influence of uneven sampling of climate space and
185 weighting the contribution of individual taxa according to their climate tolerances (Liu et al.,
186 2020). Version 2 of f_x TWA-PLS (f_x TWA-PLSv2: Liu et al., 2023) uses P-splines smoothing
187 to derive the frequency correction and applies this correction both in estimating the climate

188 optima and tolerances, and in the regression itself, producing a further improvement in model
189 performance compared to $fxTWA-PLSv1$ (Liu et al., 2020).

190 We choose $fxTWA-PLSv2$ here. The evaluation is made by comparing the reconstructions made
191 using modern pollen data with modern climates using leave-out cross-validation, where one
192 site at a time is randomly selected as a test site and sites that are both geographically close
193 (within 50 km horizontal distance from the site) and climatically close (within 2% of the full
194 range of each climate variable in the dataset) are also removed from the training set, to prevent
195 redundancy in the climate information from inflating the cross-validation goodness of fit,
196 following Liu et al. (2020). This ensures that we are not just tuning to the training dataset, and
197 that we can reconstruct climates even when the training set does not completely cover the
198 climate to be reconstructed because there are gaps in the climate space. Performance is assessed
199 using R^2 and RMSEP (root-mean-square error of prediction), and compression is assessed
200 using linear regression of the leave-out cross-validated reconstructions against the climate
201 variable. The last significant number of components ($p \leq 0.01$) is selected to avoid overfitting
202 due to the increase in the number of components. Reconstructions of MTCO, MTWA and α_{plant}
203 are then made for every sample in each fossil record, using the last significant number of
204 components. Sample-specific errors are estimated via bootstrapping (resampling the training
205 set 1000 times) as described in Liu et al. (2020).

206 However, the low CO_2 at glacial period could lead to potential bias between reconstructed and
207 actual plant-available moisture. Atmospheric CO_2 concentration has a direct impact on plant
208 physiological processes, by modulating water-use efficiency (WUE), that is the ratio of carbon
209 uptake to water loss through the stomata (Hatfield and Dold, 2019). The low CO_2 during the
210 glacial period led to reduced water use efficiency (Farquhar, 1997; Gerhart and Ward, 2010;
211 Prentice and Harrison, 2009). Strictly statistical reconstructions cannot take this into account
212 since they are based on modern relationships between pollen assemblages and climate under
213 recent CO_2 levels (Bartlein et al., 2011; Chevalier et al., 2020). Reconstructions based on
214 inversion of a vegetation model (e.g. Garreta et al., 2010; Guiot et al., 2000; Izumi and Bartlein,
215 2016; Wu et al., 2007) implicitly account for the impact of CO_2 on vegetation composition, but
216 the reconstructions are dependent on the reliability of the vegetation model and its sensitivity
217 to CO_2 changes (Chevalier et al., 2020; Guiot et al., 2009). The actual conditions under low
218 CO_2 should be wetter than the vegetation-based reconstructions of moisture variables (Prentice
219 et al., 2017, 2022a). Prentice et al. (2022a) provide a correction method to account for

220 variations on CO₂ based on combining eco-evolutionary optimality theory and experimental
 221 evidence on how the water-use efficiency as expressed by the ratio of leaf-internal to ambient
 222 CO₂ responds to variations in CO₂, as follows:

$$223 \quad e(MTGR_1, MI_1, c_{a1}) = e(MTGR_0, MI_0, c_{a0}) \quad (1)$$

224 where e is the ratio of water loss to CO₂ uptake, a function of the mean temperature of the
 225 growing season (MTGR), moisture index (MI) and atmospheric CO₂ concentration (c_a). For
 226 MTGR and c_a , the subscript “1” denotes the past value, and the subscript “0” denotes the
 227 modern value. MI₀ is the reconstructed uncorrected past value, MI₁ is the “true” past value (to
 228 be estimated). The equation means that the “true” MI under past atmospheric conditions should
 229 produce the same e with the reconstructed uncorrected MI under modern atmospheric
 230 conditions, i.e. those pertaining to the modern pollen calibration dataset.

231 We transfer our reconstructed past α_{plant} back to the uncorrected moisture index MI₀, and apply
 232 the CO₂ correction to obtain the actual moisture index MI₁, then transfer it to actual plant-
 233 available moisture $\alpha_{\text{plant,corrected}}$ (Figure 2; Figures S2-1 & S2-2). Past and modern values of CO₂
 234 concentrations are taken from Bereiter et al. (2015), following Prentice et al. (2022a). Past
 235 MTGR values are inferred by sinusoidal interpolation of reconstructed MTCO and MTWA,
 236 assuming that the growing season corresponds to the period with temperatures > 0°C. Modern
 237 MTGR values are obtained using a geographically-weighted regression (GWR) of
 238 climatological values (1961-1990) from the Climatic Research Unit Time-Series version 4.04
 239 (CRU TS4.04; Harris et al., 2020) dataset averaged over the period 1961–1990, in order to
 240 correct for elevation differences between the CRU grid cells and the fossil pollen sites. The
 241 elevations of marine sites are set to 0 when applying GWR.

242 The CO₂ correction is implemented through the package COdos 0.0.2 (Prentice et al., 2022b)
 243 with one modification, as follows. We found when applying the correction in cases where the
 244 temperature reduction from modern was large (> 5°C) that the use of different temperature
 245 values to calculate the stomatal sensitivity term (ξ) and the compensation point (Γ^*) in the
 246 correction algorithm sometimes produced an unrealistically large countervailing effect due to
 247 the temperature difference alone. To avoid this problem, we calculate these physiological
 248 quantities (ξ and Γ^*) using the mean of MTGR₁ and MTGR₀.

249 2.3. Age modelling of fossil records

250 Both the ACER and ACER2 database provide age models for each pollen record. However,
251 the resolutions of the individual records are variable (ranging from 57 years to 13415 years)
252 and these age models are often imperfectly aligned with the dating of D-O warming events as
253 recorded in the Greenland ice core, and which have been shown to have a globally synchronous
254 imprint through analysis of speleothem records (Adolphi et al., 2018; Corrick et al., 2020). To
255 create a better alignment, we use dynamic time warping (DTW: Alshehri et al., 2019; Burstyn
256 et al., 2021; Giorgino, 2009) to adjust the age scale for each individual terrestrial record (Figure
257 2). Dynamic time warping optimises the similarity between two sequences (one “query” and
258 one “reference”) by stretching or compressing one sequence in the time dimension to match
259 the other. It adjusts the age scale without influencing the variable values, thus retaining the
260 original amplitude of change.

261 LOVECLIM simulation (Menviel et al., 2014) (covering the interval 50-30 ka) is currently the
262 only published simulation that has attempted to reproduce the specific timing and magnitude
263 of successive D-O cycles. It is coupled ocean-atmosphere-vegetation general circulation model
264 of intermediate complexity. The model was spun up to equilibrium using an initial atmospheric
265 CO₂ concentration of 207.5 ppm, orbital forcing appropriate for 50 ka BP, and an estimate of
266 the 50 ka BP ice-sheet orography and albedo obtained from an off-line ice-sheet model
267 simulation (Abe-Ouchi et al., 2007). After this initialization, the model was forced by time-
268 varying changes in orbital parameters, atmospheric trace gas concentrations and ice-sheet
269 configurations following Timm et al. (2008). In addition, meltwater pulses were added in the
270 North Atlantic in such a way as to reproduce observed sea-surface temperature (SST) variations
271 along the Iberian margin (Martrat et al., 2007). The simulations have proved adequate to
272 capture at least broad features of actual D-O events, and generally consistent with the
273 qualitative signals in Voelker (2002) compilation (Liu et al., 2022). We convert the age scale
274 of LOVECLIM simulations to match the Antarctic Ice Core Chronology 2012 (AICC2012)
275 time scale (Veres et al., 2013).

276 We treat the mean annual temperature (MAT) calculated as the average of MTCO and MTWA
277 reconstructed from each individual fossil pollen record as the “query” time series, and find the
278 corresponding grid cell (the location of this fossil pollen record) in LOVECLIM simulations,
279 and use the simulated MAT at this grid cell as the “reference” time series. We further divide
280 each “query” and “reference” time series into discrete intervals using the mid-points between

281 the start dates of each D-O warming event as recorded in the Greenland ice core (Wolff et al.,
 282 2010; converted into AICC2012 timescale), and normalize both time series in each interval to
 283 remove the influence of differences in absolute values and the amplitude of changes. Then we
 284 apply dynamic time warping to modify the time scale of the “query” to match the “reference”
 285 in each interval. The adjusted age model for each fossil record is then applied to the
 286 reconstructions of MTCO, MTWA, α_{plant} and $\alpha_{\text{plant,corrected}}$ from that record for subsequent
 287 analyses.

288 **2.4. Assessment of regional climate changes during Greenland D-O warming events**

289 The magnitude of climate change during the interval corresponding to each D-O warming event
 290 as registered in Greenland is calculated individually for each climate variable at each site. To
 291 avoid making an assumption about the sign of the climate change at a site, we use a third-order
 292 polynomial to fit the reconstructions during the interval from 300 years before to 600 years
 293 after the official start date corresponding to Greenland D-O warming for each event (Wolff et
 294 al., 2010; converted into AICC2012 timescale) to determine whether the change was positive
 295 or negative. We then find the ages where this polynomial curve reaches the minimum and
 296 maximum ($t_{\text{min,polynomial}}$ and $t_{\text{max,polynomial}}$). Since the smoothed polynomial may underestimate
 297 or overestimate the amplitude of change, we use the reconstructions corresponding to
 298 $t_{\text{min,polynomial}}$ and $t_{\text{max,polynomial}}$ to obtain the changes (see Figure S3 for illustration). Whether it’s
 299 an increasing or decreasing signal depends on whether $t_{\text{min,polynomial}}$ occurs before or after
 300 $t_{\text{max,polynomial}}$. The change of each climate variable (ΔV) is calculated as:

$$301 \quad \Delta V = V_{\text{end}} - V_{\text{start}} \quad (2)$$

302 where V_{start} is the reconstructed value at the start and V_{end} is the reconstructed value at the end
 303 of the event. The error of change ($\sigma_{\Delta V}$) is calculated using the following equation assuming
 304 V_{start} and V_{end} are independent:

$$305 \quad \sigma_{\Delta V} = \sqrt{\sigma_{V_{\text{end}}}^2 + \sigma_{V_{\text{start}}}^2} \quad (3)$$

306 where $\sigma_{V_{\text{start}}}$ is the sample-specific error of V_{start} and $\sigma_{V_{\text{end}}}$ is the sample-specific error of V_{end} .

307 To obtain the relationships between changes in different climate variables, we use a maximum
308 likelihood method to estimate the ratio of ΔMTCO to ΔMTWA and the ratio of $\Delta\alpha_{\text{plant,corrected}}$
309 to ΔMTWA to take account of the errors on both variables, following Liu et al. (2022).

310 As a measure of the accuracy of the DTW method to identify D-O events, we compare the
311 number of identified events with the number of D-O events that should occur during the time
312 covered by each record (Table 1). To assess whether events are missed in a particular record
313 due to low sampling resolution, we examine the number of samples present in the 900-year
314 interval covering the sampled D-O (i.e. 300 years before to 600 years after the official start
315 date corresponding to Greenland D-O warming for each event), where low resolution is defined
316 as ≤ 3 samples in this 900-year interval.

317 **3. Results**

318 fxTWA-PLS reproduces the modern climate reasonably well (Table 2; Figures S4-1 & 4-2).
319 The performance is best for MTCO ($R^2 = 0.74$, RMSEP = 6.66, slope = 0.84) but is also good
320 for MTWA ($R^2 = 0.60$, RMSEP = 3.63, slope = 0.72) and α_{plant} ($R^2 = 0.63$, RMSEP = 0.186,
321 slope = 0.68). Assessment of the variance inflation factor scores shows that there is no problem
322 of multicollinearity so that it is possible to reconstruct all three climate variables independently
323 (Supplementary Table 1).

324 The use of dynamic time warping makes it possible to identify D-O events robustly (Figures
325 S5-1 to S5-8; Table 1; Supplementary Table 2). Some sites provide records in 50-30 ka but do
326 not cover the intervals of the D-O events; some marine sites are too far from the land to extract
327 GWR modern MTGR to apply CO_2 correction. Across the remaining 179 sites which should
328 have D-O events registered, we have identified 544 out of the 696 individual events (78 %). In
329 the majority of cases where a D-O event should have been registered but could not be identified
330 in an individual record (134 out of 152 cases), the resolution of that part of the record is
331 extremely poor.

332 ΔMTCO is found to be significantly larger than ΔMTWA in the northern extratropics and
333 tropics when considered across all D-O events and sites, indicating reduced seasonal contrast
334 between winter and summer temperatures; ΔMTCO is found to be larger than ΔMTWA , but
335 not significantly larger, in the southern extratropics (Figure 3; Table 3). There is no globally

336 consistent relationship between $\Delta\alpha_{\text{plant,corrected}}$ and ΔMTWA , although the positive relationship
337 in the tropics is marginally significant (Figure 4; Table 4).

338 The spatial patterns of ΔMTCO and ΔMTWA are generally consistent across multiple D-O
339 events (Figure 5), most noticeably that the largest warming occurs in Eurasia, while western
340 North America and the southern extratropics are characterised by cooling. These patterns are
341 also shown if only reconstructions where the change is twice the error of change are considered
342 (Figure S6), proving that the spatial patterns are robust to the choice of threshold. Nevertheless,
343 both the magnitude of the changes and the spatial patterns vary between the D-O events
344 (Figures S7-1 & S7-2). Strong events such as D-O 8 show more apparent changes (whether
345 warming or cooling), as well as a strong antiphasing between northern and southern
346 extratropical changes; while weak events such as D-O 9 show less apparent changes with
347 almost no north-south antiphasing (Figure 6).

348 The changes in plant-available moisture are less spatially coherent than the changes in
349 temperature (Figure 5). There is an increase in $\alpha_{\text{plant,corrected}}$ in some regions characterised by
350 warming, for example, southeastern China and Japan; but there are mixed signals of drying and
351 wetting in other regions characterised by warming, such as southern Europe. Furthermore,
352 regions characterised by cooling, such as western North America and southern extratropics,
353 can also show both drying and wetting. Changes in $\Delta\alpha_{\text{plant,corrected}}$ also show more variability
354 between D-O events than changes in temperature (Figure S7-4). We have applied a correction
355 for low CO_2 values during the glacial period to plant-available moisture. The actual values
356 ($\alpha_{\text{plant,corrected}}$) are generally higher than the vegetation-based reconstructed values (α_{plant})
357 (Figure S2-1). However, the correction does not have a significant impact on the spatial
358 patterns during D-O events (Figure S2-2; Figure S7-3).

359 **4. Discussion and Conclusions**

360 **4.1. Comparison with previous reconstructions**

361 We have presented a first attempt to map the spatial patterns of quantitative changes in seasonal
362 temperatures and plant-available moisture during D-O events globally, using a consistent
363 methodology. These analyses show that there is an anti-phasing between changes in the
364 northern extratropics and the southern extratropics, with warming in the north and cooling in
365 the south. The largest and most consistent warming during D-O events occurs in Eurasia. There

366 is a significant difference between winter warming and summer warming in the northern
367 extratropics, resulting in an overall reduction in seasonality. Site-based reconstructions from
368 the Eifel region in central Europe, based on branched glycerol dialkyl glycerol tetraethers,
369 indicate minimal temperature changes during summer (Zander et al., 2024) and thus support
370 the idea that the D-O changes were driven by large changes in winter temperature. Zumaque
371 et al., (2025) provide seasonal temperature and precipitation reconstructions for 12 of the sites
372 from southern Europe (which are included in our fossil pollen records) but using the modern
373 analogue technique as the reconstruction method and the Eurasian Modern Pollen Database
374 version 2 (Davis et al., 2020) (EMPDv2; also included in our SMPDSv3) as the modern
375 training dataset. They show relatively stable summer temperatures but large change in MTCO
376 through the MIS3 D-O events, consistent with our reconstructions (using a regression-based
377 reconstruction method and a global modern training dataset) of a reduction in seasonality
378 during warming events in the northern extratropics. We find no significant difference in the
379 magnitude of seasonal warming in the southern extratropics. Since only quantitative
380 reconstructions of MAT (rather than MTCO and MTWA) are available from the southern
381 extratropics (e.g. Fletcher and Thomas, 2010; Newnham et al., 2017), there is no independent
382 confirmation of this result.

383 Qualitative interpretation of palaeo-records suggest that many regions are characterised by both
384 warming and wetting, such as western Europe (Fletcher et al., 2010; Sánchez-Goñi et al., 2008),
385 eastern Europe (Fleitmann et al., 2009; Stockhecke et al., 2016), central Siberia (Grygar et al.,
386 2006), and the Great Basin USA (Denniston et al., 2007; Jiménez-Moreno et al., 2010).
387 Previous studies have also indicated drier conditions during D-O events, particularly in parts
388 of the USA such as the Pacific Northwest (Grigg and Whitlock, 2002) and Florida (Grimm et
389 al., 2006; Jiménez-Moreno et al., 2010). Our reconstructions show more mixed signals and that
390 there is no globally consistent relationship between changes in temperature and moisture, either
391 in regions characterised by warming or by cooling (Figure 4; Figure 5).

392 **4.2. Global training dataset vs local training dataset**

393 We have used a global pollen dataset for calibration of the pollen-climate relationships. In
394 general, reconstructions of glacial climates have used region-specific data sets (e.g. Dugerdil
395 et al., 2021, 2025; Newnham et al., 2017; Wei et al., 2021; Zumaque et al., 2025). Herzschuh
396 et al. (2023) made this explicit in their reconstructions of northern hemisphere climate over the

397 past 30,000 years, by restricting the modern training data to within a 2000 km radius of
398 individual fossil sites. The use of a region-specific training data set can be justified on the
399 grounds that it produces better statistics for the modern-day relationship between pollen
400 abundance and specific climate variables. Nevertheless, as pointed out by Chevalier et al.
401 (2020), an important issue is that the modern calibration data set has a span that adequately
402 samples the climate space experienced in the past. The use of a global dataset for calibration
403 makes it possible to sample a larger range of climates, and specifically to reconstruct climates
404 that might be very different from the modern range in that region. For example, reconstructions
405 of past European climate (Figure S8) based on region-specific training dataset would yield less
406 extreme winter temperatures than reconstructed using the global training data set. Although the
407 trend and spatial pattern might not be influenced greatly, the amplitude of change might be
408 underestimated.

409 The use of a global dataset, rather than region-specific training data, relies on the principle of
410 phylogenetic niche conservatism (Harvey and Pagel, 1991; Qian and Ricklefs, 2004; Wang et
411 al., 2025), which states that traits tend to remain constant over time. This also applies to the
412 climate niche (Crisp and Cook, 2012; Jiang et al., 2023; Peterson, 2011; Wiens et al., 2010;
413 Wiens and Graham, 2005) as evidenced by disjunct distributions of taxa across different
414 continents (Yin et al., 2021). Niche conservatism underpins the fact that the modern
415 distribution of specific genera can be predicted using climate-pollen relationships developed
416 from other regions (e.g. Huntley et al., 1989). However, the use of a global dataset can create
417 issues because of inconsistencies in taxonomic resolution between regions. The necessity for
418 treating all species of *Quercus* as a single taxon, despite the fact that evergreen and deciduous
419 species may occupy distinct climate niches in some regions, is a consequence of this. However,
420 we have shown (Supplementary Materials, section 4) that this has little impact on our
421 reconstructions – largely because the climatic distinction that would be conveyed through
422 separating deciduous and evergreen *Quercus* is also registered by the presence of other taxa.
423 Although the use of a global training dataset for climate reconstructions has not been a common
424 practice, it addresses the need to ensure that the modern training data adequately represents
425 past climate conditions and also facilitates making reconstructions for sites from regions with
426 limited modern pollen data.

427 4.3. Targets for model evaluation

428 The reconstructions in this paper can be used as targets for model evaluation, specifically the
429 two transient D-O experiments planned for the next phase of the Palaeoclimate Modelling
430 Intercomparison (see Malmierca-Vallet et al., 2023 for the experimental protocol). The first of
431 these experiments is a baseline simulation starting at 34 ka, a time with low obliquity, moderate
432 MIS3 greenhouse gas values, and an intermediate ice sheet configuration, which appears to be
433 most conducive to generating D-O like behaviour in climate models. The second experiment
434 involves the addition of freshwater, to examine whether this is necessary to precondition a state
435 conducive to generating D-O events. The anti-phasing in reconstructed temperature changes
436 between the northern and southern hemispheres is a general feature of climate model
437 experiments. Most models show larger warming in winter than in summer in the northern
438 hemisphere (e.g. Flückiger et al., 2008; Izumi et al., 2023; Van Meerbeeck et al., 2011), which
439 is also consistent with our reconstructions. However, the cooling in western North America
440 during D-O warming events in our reconstructions is not a feature of all climate model
441 simulations.

442 Models generally show an intensification of the northern hemisphere monsoons during D-O
443 events (e.g. Izumi et al., 2023; Menviel et al., 2020), but there is less consistency about changes
444 in plant-available moisture in the extratropics. Our reconstructions show an increase in
445 $\alpha_{\text{plant,corrected}}$ in southeastern China and Japan (Figure 5). Although $\alpha_{\text{plant,corrected}}$ is not a direct
446 reflection of summer precipitation, these changes are consistent with enhanced northern
447 hemisphere monsoons during D-O warming events, as shown by speleothem records from the
448 Caribbean (Warren et al., 2019) and speleothem and pollen records from Asia (Fohlmeister et
449 al., 2023; Wang et al., 2001; Zorzi et al., 2022). However, there are more spatial variability and
450 mixed signals.

451 The LOVECLIM model was used as a reference to adjust the age scale in the reconstructions
452 using MAT, but this does not preclude comparison of the seasonal temperatures. Here we
453 approximate the winter-season temperature as MTCO and summer-season temperature as
454 MTWA, since monthly temperatures are not available (only seasonal temperatures are available)
455 in LOVECLIM. The general spatial pattern of simulated changes in MTCO and MTWA (Figure
456 7) is consistent with the reconstructions, with largest warming in Eurasia, and cooling in the
457 southern extratropics. The simulated changes are strong during D-O 8 but weak during D-O 9
458 (Figures 9-1 & 9-2), again as shown by the reconstructions. However, there are important

459 differences. For example, simulated changes generally have smaller amplitude than shown by
460 the reconstructions, and the cooling over western North America is generally only in winter,
461 while the reconstructions show cooling over this region in both seasons. The relationship
462 between ΔMTCO and ΔMTWA is also different (Figure 8; Table 5): the simulated ΔMTCO is
463 shown to be significantly larger than ΔMTWA in the northern extratropics, but significantly
464 smaller than ΔMTWA in the southern extratropics, a contrast that is not so marked in the
465 reconstructions. This comparison illustrates the usefulness of the reconstructions for model
466 evaluation and to investigate the mechanisms that may not be adequately captured by current
467 models.

468 **4.4. Implications of the use of dynamic time warping**

469 Identifying D-O events in pollen records is often problematic, particularly in regions where
470 warming (especially if accompanied by dryer conditions) leads to a reduction (or an hiatus) in
471 sedimentation as reflected in the variable resolution of the available pollen records (e.g.
472 Camuera et al., 2022; Pini et al., 2022; Sinopoli et al., 2019; Wei et al., 2021). The use of
473 dynamic time warping goes some way to improving the identification of potential D-O events.
474 However, it precludes the calculation of a rate of change in climate. Thus, we have focused
475 here on the magnitude of the changes during specific warming events. It is also likely that some
476 of the variability in the reconstructed changes between different D-O events reflects imperfect
477 identification of specific events because of the comparatively modest resolution of the records.

478

479 **Data and code availability.** Data and codes used in this paper are available at
480 <https://doi.org/10.5281/zenodo.18218890>.

481 **Author contributions.** ML, SPH and ICP designed the study. ML made the reconstructions
482 and produced the figures and tables. ML and SPH carried out the analyses. SPH wrote the first
483 draft of the paper and all authors contributed to the final draft.

484 **Competing Interests.** The authors declare not competing interests.

485 **Acknowledgements.** ML acknowledges support from Imperial College through the Lee
486 Family Scholarship. ICP acknowledges support from the ERC under the European Union
487 Horizon 2020 research and innovation programme (grant agreement no.: 787203 REALM).

488 SPH acknowledges fruitful discussions with colleagues from the D-O community working
489 group. We would like to acknowledge our colleagues who provided original pollen data for
490 inclusion in the ACER2 data set: Jon Camuera, Penelope González-Sampériz, Gonzalo
491 Jiménez-Moreno, Xinghi Liu, Rewi Newnham, Jian Ni, Roberta Pini, Cassie Rowe, Frank
492 Sirocco and María Del Socorro Lozano-García.

493

494

495 **References**

- 496 Abe-Ouchi, A., Segawa, T. and Saito, F.: Climatic conditions for modelling the Northern
497 Hemisphere ice sheets throughout the ice age cycle, *Clim. Past*, 3(3), 423–438,
498 doi:10.5194/cp-3-423-2007, 2007.
- 499 Adolphi, F., Bronk Ramsey, C., Erhardt, T., Edwards, R. L., Cheng, H., Turney, C. S. M.,
500 Cooper, A., Svensson, A., Rasmussen, S. O., Fischer, H. and Muscheler, R.: Connecting the
501 Greenland ice-core and U/Th timescales via cosmogenic radionuclides: testing the
502 synchronicity of Dansgaard–Oeschger events, *Clim. Past*, 14(11), 1755–1781, doi:10.5194/cp-
503 14-1755-2018, 2018.
- 504 Alshehri, M., Coenen, F. and Dures, K.: Effective sub-sequence-based dynamic time
505 warping, in *Artificial Intelligence XXXVI. SGAI 2019. Lecture Notes in Computer Science*,
506 edited by M. Bramer and M. Petridis, p. 11927, Springer, Cham., 2019.
- 507 Ampel, L., Bigler, C., Wohlfarth, B., Risberg, J., Lotter, A. F. and Veres, D.: Modest summer
508 temperature variability during DO cycles in western Europe, *Quat. Sci. Rev.*, 29(11), 1322–
509 1327, doi:10.1016/j.quascirev.2010.03.002, 2010.
- 510 Bartlein, P. J., Harrison, S. P., Brewer, S., Connor, S., Davis, B. A. S., Gajewski, K., Guiot,
511 J., Harrison-Prentice, T. I., Henderson, A., Peyron, O., Prentice, I. C., Scholze, M., Seppä, H.,
512 Shuman, B., Sugita, S., Thompson, R. S., Viau, A. E., Williams, J. and Wu, H.: Pollen-based
513 continental climate reconstructions at 6 and 21 ka: A global synthesis, *Clim. Dyn.*, 37(3),
514 775–802, doi:10.1007/s00382-010-0904-1, 2011.
- 515 Bereiter, B., Eggleston, S., Schmitt, J., Nehrbass-Ahles, C., Stocker, T. F., Fischer, H.,
516 Kipfstuhl, S. and Chappellaz, J.: Revision of the EPICA Dome C CO₂ record from 800 to 600
517 kyr before present, *Geophys. Res. Lett.*, 42(2), 542–549, doi:10.1002/2014GL061957, 2015.
- 518 Boucher-Lalonde, V., Morin, A. and Currie, D. J.: How are tree species distributed in
519 climatic space? A simple and general pattern, *Glob. Ecol. Biogeogr.*, 21(12), 1157–1166,
520 doi:10.1111/j.1466-8238.2012.00764.x, 2012.
- 521 Burstyn, Y., Gazit, A. and Dvir, O.: Hierarchical dynamic time warping methodology for
522 aggregating multiple geological time series, *Comput. Geosci.*, 150, 104704,
523 doi:10.1016/j.cageo.2021.104704, 2021.

- 524 Camuera, J., Ramos-Román, M. J., Jiménez-Moreno, G., García-Alix, A., Ilvonen, L., Ruha,
525 L., Gil-Romera, G., González-Sampériz, P. and Seppä, H.: Past 200 kyr hydroclimate
526 variability in the western Mediterranean and its connection to the African Humid Periods,
527 *Sci. Rep.*, 12(1), 9050, doi:10.1038/s41598-022-12047-1, 2022.
- 528 Cao, X., Tian, F., Andreev, A. A., Anderson, P. M., Lozhkin, A. V, Bezrukova, E. V, Ni, J.,
529 Rudaya, N., Stobbe, A., Wieczorek, M. and Herzsuh, U.: A taxonomically harmonized and
530 temporally standardized fossil pollen dataset from Siberia covering the last 40 ka [dataset
531 publication series], PANGAEA, doi:10.1594/PANGAEA.898616, 2019.
- 532 Cao, X., Tian, F., Andreev, A., Anderson, P. M., Lozhkin, A. V, Bezrukova, E., Ni, J.,
533 Rudaya, N., Stobbe, A., Wieczorek, M. and Herzsuh, U.: A taxonomically harmonized and
534 temporally standardized fossil pollen dataset from Siberia covering the last 40 kyr, *Earth
535 Syst. Sci. Data*, 12(1), 119–135, doi:10.5194/essd-12-119-2020, 2020.
- 536 Chevalier, M., Davis, B. A. S., Heiri, O., Seppä, H., Chase, B. M., Gajewski, K., Lacourse,
537 T., Telford, R. J., Finsinger, W., Guiot, J., Köhl, N., Maezumi, S. Y., Tipton, J. R., Carter, V.
538 A., Brussel, T., Phelps, L. N., Dawson, A., Zanon, M., Vallé, F., Nolan, C., Mauri, A., de
539 Vernal, A., Izumi, K., Holmström, L., Marsicek, J., Goring, S., Sommer, P. S., Chaput, M.
540 and Kupriyanov, D.: Pollen-based climate reconstruction techniques for late Quaternary
541 studies, *Earth-Science Rev.*, 210, 103384, doi:10.1016/j.earscirev.2020.103384, 2020.
- 542 Corrick, E. C., Drysdale, R. N., Hellstrom, J. C., Capron, E., Rasmussen, S. O., Zhang, X.,
543 Fleitmann, D., Couchoud, I. and Wolff, E.: Synchronous timing of abrupt climate changes
544 during the last glacial period, *Science (80-.)*, 369(6506), 963 LP – 969,
545 doi:10.1126/science.aay5538, 2020.
- 546 Crisp, M. D. and Cook, L. G.: Phylogenetic niche conservatism: What are the underlying
547 evolutionary and ecological causes?, *New Phytol.*, 196(3), 681–694, doi:10.1111/j.1469-
548 8137.2012.04298.x, 2012.
- 549 Dansgaard, W., Johnsen, S. J., Clausen, H. B., Dahl-Jensen, D., Gundestrup, N. S., Hammer,
550 C. U., Hvidberg, C. S., Steffensen, J. P., Sveinbjörnsdottir, A. E., Jouzel, J. and Bond, G.:
551 Evidence for general instability of past climate from a 250-kyr ice-core record, *Nature*,
552 364(6434), 218–220, doi:10.1038/364218a0, 1993.

- 553 Davis, B. A. S., Chevalier, M., Sommer, P., Carter, V. A., Finsinger, W., Mauri, A., Phelps,
554 L. N., Zanon, M., Abegglen, R., Åkesson, C. M., Alba-Sánchez, F., Anderson, R. S.,
555 Antipina, T. G., Atanassova, J. R., Beer, R., Belyanina, N. I., Blyakharchuk, T. A., Borisova,
556 O. K., Bozilova, E., Bukreeva, G., Bunting, M. J., Clò, E., Colombaroli, D., Combourieu-
557 Nebout, N., Desprat, S., Di Rita, F., Djamali, M., Edwards, K. J., Fall, P. L., Feurdean, A.,
558 Fletcher, W., Florenzano, A., Furlanetto, G., Gaceur, E., Galimov, A. T., Gałka, M.,
559 Garcia-Moreiras, I., Giesecke, T., Grindean, R., Guido, M. A., Gvozdeva, I. G., Herzs Schuh,
560 U., Hjelle, K. L., Ivanov, S., Jahns, S., Jankovska, V., Jiménez-Moreno, G., Karpińska-
561 Kołaczek, M., Kitaba, I., Kołaczek, P., Lapteva, E. G., Latałowa, M., Lebreton, V., Leroy, S.,
562 Leydet, M., Lopatina, D. A., López-Sáez, J. A., Lotter, A. F., Magri, D., Marinova, E.,
563 Matthias, I., Mavridou, A., Mercuri, A. M., Mesa-Fernández, J. M., Mikishin, Y. A.,
564 Milecka, K., Montanari, C., Morales-Molino, C., Mrotzek, A., Muñoz Sobrino, C., Naidina,
565 O. D., Nakagawa, T., Nielsen, A. B., Novenko, E. Y., Panajiotidis, S., Panova, N. K.,
566 Papadopoulou, M., Pardoe, H. S., Pędziszewska, A., Petrenko, T. I., Ramos-Román, M. J.,
567 Ravazzi, C., Rösch, M., Ryabogina, N., Sabariego Ruiz, S., Salonen, J. S., Sapelko, T. V.,
568 Schofield, J. E., Seppä, H., Shumilovskikh, L., Stivrins, N., Stojakowits, P., Svobodova
569 Svitavska, H., Świąta-Musznicka, J., Tantau, I., Tinner, W., Tobolski, K., Tonkov, S.,
570 Tsakiridou, M., et al.: The Eurasian Modern Pollen Database (EMPD), Version 2, Earth Syst.
571 Sci. Data Discuss., 2020, 1–41, doi:10.5194/essd-2020-14, 2020.
- 572 Davis, T. W., Prentice, I. C., Stocker, B. D., Thomas, R. T., Whitley, R. J., Wang, H., Evans,
573 B. J., Gallego-Sala, A. V., Sykes, M. T. and Cramer, W.: Simple process-led algorithms for
574 simulating habitats (SPLASH v.1.0): Robust indices of radiation, evapotranspiration and
575 plant-available moisture, *Geosci. Model Dev.*, 10(2), 689–708, doi:10.5194/gmd-10-689-
576 2017, 2017.
- 577 Denniston, R. F., Asmerom, Y., Polyak, V., Dorale, J. A., Carpenter, S. J., Trodick, C., Hoye,
578 B. and González, L. A.: Synchronous millennial-scale climatic changes in the Great Basin
579 and the North Atlantic during the last interglacial, *Geology*, 35(7), 619–622,
580 doi:10.1130/G23445A.1, 2007.
- 581 Dima, M., Lohmann, G. and Knorr, G.: North Atlantic versus global control on Dansgaard-
582 Oeschger events, *Geophys. Res. Lett.*, 45(23), 12,912–991,998, doi:10.1029/2018GL080035,
583 2018.

- 584 Doblus-Reyes, F. J., Sörensson, A. A., Almazroui, M., Dosio, A., Gutowski, W. J., Haarsma,
585 R., Hamdi, R., Hewitson, B., Kwon, W.-T., Lamptey, B. L., Maraun, D., Stephenson, T. S.,
586 Takayabu, I., Terray, L., Turner, A. and Zuo, Z.: Linking global to regional climate change,
587 in *Climate Change 2021 – The Physical Science Basis: Working Group I Contribution to the*
588 *Sixth Assessment Report of the Intergovernmental Panel on Climate Change*, edited by V.
589 Masson-Delmotte, P. Zhai, A. Pirani, S. L. Connors, C. Péan, S. Berger, N. Caud, Y. Chen, L.
590 Goldfarb, M. I. Gomis, M. Huang, K. Leitzell, E. Lonnoy, J. B. R. Matthews, T. K. Maycock,
591 T. Waterfield, O. Yelekçi, R. Yu, and B. Zhou, pp. 1363–1512, Cambridge University Press,
592 Cambridge, United Kingdom and New York, NY, USA., 2021.
- 593 Dugerdil, L., Joannin, S., Peyron, O., Jouffroy-Bapicot, I., Vannière, B., Boldgiv, B.,
594 Unkelbach, J., Behling, H. and Ménot, G.: Climate reconstructions based on GDGT and
595 pollen surface datasets from Mongolia and Baikal area: calibrations and applicability to
596 extremely cold–dry environments over the Late Holocene, *Clim. Past*, 17(3), 1199–1226,
597 doi:10.5194/cp-17-1199-2021, 2021.
- 598 Dugerdil, L., Peyron, O., Ménot, G., Egamberdieva, D., Alimov, J., Leroy, S. A. G., Garnier,
599 E., Nowak, A. and Joannin, S.: First paleoenvironmental calibrations for modern pollen rain
600 of Tajikistan and Uzbekistan: A case study of pollen - vegetation functional biogeography of
601 Arid Central Asia, *Glob. Planet. Change*, 252, 104857, doi:10.1016/j.gloplacha.2025.104857,
602 2025.
- 603 Farquhar, G. D.: Carbon dioxide and vegetation, *Science* (80-.), 278(5342), 1411,
604 doi:10.1126/science.278.5342.1411, 1997.
- 605 Fleitmann, D., Cheng, H., Badertscher, S., Edwards, R. L., Mudelsee, M., Göktürk, O. M.,
606 Fankhauser, A., Pickering, R., Raible, C. C., Matter, A., Kramers, J. and Tüysüz, O.: Timing
607 and climatic impact of Greenland interstadials recorded in stalagmites from northern Turkey,
608 *Geophys. Res. Lett.*, 36(19), doi:10.1029/2009GL040050, 2009.
- 609 Fletcher, M.-S. and Thomas, I.: A quantitative Late Quaternary temperature reconstruction
610 from western Tasmania, Australia, *Quat. Sci. Rev.*, 29(17), 2351–2361,
611 doi:10.1016/j.quascirev.2010.06.012, 2010.
- 612 Fletcher, W. J., Sánchez-Goñi, M. F., Allen, J. R. M., Cheddadi, R., Combourieu-Nebout, N.,
613 Huntley, B., Lawson, I., Londeix, L., Magri, D., Margari, V., Müller, U. C., Naughton, F.,

- 614 Novenko, E., Roucoux, K. and Tzedakis, P. C.: Millennial-scale variability during the last
615 glacial in vegetation records from Europe, *Quat. Sci. Rev.*, 29(21), 2839–2864,
616 doi:10.1016/j.quascirev.2009.11.015, 2010.
- 617 Flückiger, J., Knutti, R., White, J. W. C. and Renssen, H.: Modeled seasonality of glacial
618 abrupt climate events, *Clim. Dyn.*, 31(6), 633–645, doi:10.1007/s00382-008-0373-y, 2008.
- 619 Fohlmeister, J., Sekhon, N., Columbu, A., Vettoretti, G., Weitzel, N., Rehfeld, K., Veiga-
620 Pires, C., Ben-Yami, M., Marwan, N. and Boers, N.: Global reorganization of atmospheric
621 circulation during Dansgaard–Oeschger cycles, *Proc. Natl. Acad. Sci.*, 120(36),
622 e2302283120, doi:10.1073/pnas.2302283120, 2023.
- 623 Garreta, V., Miller, P. A., Guiot, J., Hély, C., Brewer, S., Sykes, M. T. and Litt, T.: A method
624 for climate and vegetation reconstruction through the inversion of a dynamic vegetation
625 model, *Clim. Dyn.*, 35(2), 371–389, doi:10.1007/s00382-009-0629-1, 2010.
- 626 Gerhart, L. M. and Ward, J. K.: Plant responses to low [CO₂] of the past, *New Phytol.*,
627 188(3), 674–695, doi:10.1111/j.1469-8137.2010.03441.x, 2010.
- 628 Giorgino, T.: Computing and visualizing Dynamic Time Warping alignments in R: The dtw
629 package, *J. Stat. Softw.*, 31(7 SE-Articles), 1–24, doi:10.18637/jss.v031.i07, 2009.
- 630 Grigg, L. D. and Whitlock, C.: Patterns and causes of millennial-scale climate change in the
631 Pacific Northwest during Marine Isotope Stages 2 and 3, *Quat. Sci. Rev.*, 21(18), 2067–2083,
632 doi:10.1016/S0277-3791(02)00017-3, 2002.
- 633 Grimm, E. C., Watts, W. A., Jacobson, G. L., Hansen, B. C. S., Almquist, H. R. and
634 Dieffenbacher-Krall, A. C.: Evidence for warm wet Heinrich events in Florida, *Quat. Sci.*
635 *Rev.*, 25(17), 2197–2211, doi:10.1016/j.quascirev.2006.04.008, 2006.
- 636 Grygar, T., Kadlec, J., Pruner, P., Swann, G., Bezdička, P., Hradil, D., Lang, K., Novotna, K.
637 and Oberhänsli, H.: Paleoenvironmental record in Lake Baikal sediments: Environmental
638 changes in the last 160 ky, *Palaeogeogr. Palaeoclimatol. Palaeoecol.*, 237(2), 240–254,
639 doi:10.1016/j.palaeo.2005.12.007, 2006.
- 640 Guiot, J., de Beaulieu, J. L., Cheddadi, R., David, F., Ponel, P. and Reille, M.: The climate in
641 Western Europe during the last Glacial/Interglacial cycle derived from pollen and insect

- 642 remains, *Palaeogeogr. Palaeoclimatol. Palaeoecol.*, 103(1), 73–93, doi:10.1016/0031-
643 0182(93)90053-L, 1993.
- 644 Guiot, J., Torre, F., Jolly, D., Peyron, O., Boreux, J. J. and Cheddadi, R.: Inverse vegetation
645 modeling by Monte Carlo sampling to reconstruct palaeoclimates under changed
646 precipitation seasonality and CO₂ conditions: Application to glacial climate in Mediterranean
647 region, *Ecol. Modell.*, 127(2), 119–140, doi:10.1016/S0304-3800(99)00219-7, 2000.
- 648 Guiot, J., Wu, H. B., Garreta, V., Hatté, C. and Magny, M.: A few prospective ideas on
649 climate reconstruction: From a statistical single proxy approach towards a multi-proxy and
650 dynamical approach, *Clim. Past*, 5(4), 571–583, doi:10.5194/cp-5-571-2009, 2009.
- 651 Harris, I., Osborn, T. J., Jones, P. and Lister, D.: Version 4 of the CRU TS monthly high-
652 resolution gridded multivariate climate dataset, *Sci. Data*, 7, 109, doi:10.1038/s41597-020-
653 0453-3, 2020.
- 654 Harrison, S., Egbudom, M.-A. and Villegas-Diaz, R.: The SPECIAL Modern Pollen Data Set
655 for Climate Reconstructions, version 3 (SMPDSv3), , doi:10.17864/1947.001473, 2025a.
- 656 Harrison, S. P.: Climate reconstructions for the SMPDS v1 modern pollen data set, *Univ.*
657 *Read.*, doi:10.5281/zenodo.3605003, 2020.
- 658 Harrison, S. P. and Sanchez-Goñi, M. F.: Global patterns of vegetation response to
659 millennial-scale variability and rapid climate change during the last glacial period, *Quat. Sci.*
660 *Rev.*, 29(21), 2957–2980, doi:10.1016/j.quascirev.2010.07.016, 2010.
- 661 Harrison, S. P., Egbudom, M.-A. and Liu, M.: ACER2: The Abrupt Climate Changes and
662 Environmental Responses Database (version 2), , doi:10.17864/1947.001449, 2025b.
- 663 Harrison, S. P., Bartlein, P. J., Cruz-Silva, E., Haas, O., Jackson, S. T., Kaushal, N., Liu, M.,
664 Magri, D., Robson, D., Vettoretti, G. and Prentice, I. C.: Palaeoclimate perspectives on
665 contemporary climate change, *Ann. Rev. Environ. Resour.*, 50, 2025c.
- 666 Harvey, P. H. and Pagel, M. D.: *The comparative method in evolutionary biology*, Oxford
667 University Press., 1991.
- 668 Hatfield, J. L. and Dold, C.: Water-use efficiency: Advances and challenges in a changing
669 climate, *Front. Plant Sci.*, Volume 10, doi:10.3389/fpls.2019.00103, 2019.

- 670 Herzsuh, U., Böhmer, T., Li, C., Chevalier, M., Hébert, R., Dallmeyer, A., Cao, X.,
671 Bigelow, N. H., Nazarova, L., Novenko, E. Y., Park, J., Peyron, O., Rudaya, N. A., Schlütz,
672 F., Shumilovskikh, L. S., Tarasov, P. E., Wang, Y., Wen, R., Xu, Q. and Zheng, Z.:
673 LegacyClimate 1.0: a dataset of pollen-based climate reconstructions from 2594 Northern
674 Hemisphere sites covering the last 30 kyr and beyond, *Earth Syst. Sci. Data*, 15(6), 2235–
675 2258, doi:10.5194/essd-15-2235-2023, 2023.
- 676 Huber, C., Leuenberger, M., Spahni, R., Flückiger, J., Schwander, J., Stocker, T. F., Johnsen,
677 S., Landais, A. and Jouzel, J.: Isotope calibrated Greenland temperature record over Marine
678 Isotope Stage 3 and its relation to CH₄, *Earth Planet. Sci. Lett.*, 243(3), 504–519,
679 doi:10.1016/j.epsl.2006.01.002, 2006.
- 680 Huntley, B., Bartlein, P. J. and Prentice, I. C.: Climatic control of the distribution and
681 abundance of Beech (*Fagus L.*) in Europe and North America, *J. Biogeogr.*, 16(6), 551–560,
682 doi:10.2307/2845210, 1989.
- 683 Huntley, B., Watts, W. A., Allen, J. R. M. and Zolitschka, B.: Palaeoclimate, chronology and
684 vegetation history of the Weichselian Lateglacial: comparative analysis of data from three
685 cores at Lago Grande di Monticchio, southern Italy, *Quat. Sci. Rev.*, 18(7), 945–960,
686 doi:10.1016/S0277-3791(99)00007-4, 1999.
- 687 IPCC: Climate change 2022: Impacts, adaptation and vulnerability. Contribution of working
688 group II to the sixth assessment report of the Intergovernmental Panel on Climate Change,
689 edited by H.-O. Pörtner, D. C. Roberts, M. Tignor, E. S. Poloczanska, K. Mintenbeck, A.
690 Alegría, M. Craig, S. Langsdorf, S. Löschke, V. Möller, A. Okem, and B. Rama, Cambridge
691 University Press, Cambridge University Press, Cambridge, UK and New York, NY, USA.,
692 2022.
- 693 Izumi, K. and Bartlein, P. J.: North American paleoclimate reconstructions for the Last
694 Glacial Maximum using an inverse modeling through iterative forward modeling approach
695 applied to pollen data, *Geophys. Res. Lett.*, 43(20), 10,910-965,972,
696 doi:10.1002/2016GL070152, 2016.
- 697 Izumi, K., Armstrong, E. and Valdes, P.: Global footprints of dansgaard-oeschger oscillations
698 in a GCM, *Quat. Sci. Rev.*, 305, 108016, doi:10.1016/j.quascirev.2023.108016, 2023.

- 699 Jiang, K., Wang, Q., Dimitrov, D., Luo, A., Xu, X., Su, X., Liu, Y., Li, Y., Li, Y. and Wang,
700 Z.: Evolutionary history and global angiosperm species richness–climate relationships, *Glob.*
701 *Ecol. Biogeogr.*, 32(7), 1059–1072, doi:10.1111/geb.13687, 2023.
- 702 Jiménez-Moreno, G., Anderson, R. S., Desprat, S., Grigg, L. D., Grimm, E. C., Heusser, L.
703 E., Jacobs, B. F., López-Martínez, C., Whitlock, C. L. and Willard, D. A.: Millennial-scale
704 variability during the last glacial in vegetation records from North America, *Quat. Sci. Rev.*,
705 29(21), 2865–2881, doi:10.1016/j.quascirev.2009.12.013, 2010.
- 706 Kindler, P., Guillevic, M., Baumgartner, M., Schwander, J., Landais, A. and Leuenberger,
707 M.: Temperature reconstruction from 10 to 120 kyr b2k from the NGRIP ice core, *Clim. Past*,
708 10(2), 887–902, doi:10.5194/cp-10-887-2014, 2014.
- 709 Lapellegerie, P., Millet, L., Rius, D., Duprat-Oualid, F., Luoto, T. and Heiri, O.: Chironomid-
710 inferred summer temperature during the Last Glacial Maximum in the Southern Black Forest,
711 Central Europe, *Quat. Sci. Rev.*, 345, 109016, doi:10.1016/j.quascirev.2024.109016, 2024.
- 712 Lee, J.-Y., Marotzke, J., Bala, G., Cao, L., Corti, S., Dunne, J. P., Engelbrecht, F., Fischer,
713 E., Fyfe, J. C., Jones, C., Maycock, A., Mutemi, J., Ndiaye, O., Panickal, S. and Zhou, T.:
714 Future global climate: Scenario-based projections and near-term information, in *Climate*
715 *change 2021: The physical science basis. Contribution of working group I to the sixth*
716 *assessment report of the Intergovernmental Panel on Climate Change*, edited by V. Masson-
717 Delmotte, P. Zhai, A. Pirani, S. L. Connors, C. Péan, S. Berger, N. Caud, Y. Chen, L.
718 Goldfarb, M. I. Gomis, M. Huang, K. Leitzell, E. Lonnoy, J. B. R. Matthews, T. K. Maycock,
719 T. Waterfield, O. Yelekçi, R. Yu, and B. Zhou, pp. 553–672, Cambridge University Press,
720 Cambridge, United Kingdom and New York, NY, USA., 2021.
- 721 Li, C., Ni, J., Böhmer, T., Cao, X., Zhou, B., Liao, M., Li, K., Schild, L., Wiczorek, M.,
722 Heim, B. and Herzschuh, U.: LegacyPollen2.0: an updated global taxonomically and
723 temporally standardized fossil pollen dataset of 3680 palynological records, ,
724 doi:10.1594/PANGAEA.965907, 2025.
- 725 Liu, M., Prentice, I. C., ter Braak, C. J. F. and Harrison, S. P.: An improved statistical
726 approach for reconstructing past climates from biotic assemblages, *Proc. R. Soc. A Math.*,
727 476(2243), 20200346, doi:10.1098/rspa.2020.0346, 2020.

- 728 Liu, M., Prentice, I. C., Menviel, L. and Harrison, S. P.: Past rapid warmings as a constraint
729 on greenhouse-gas climate feedbacks, *Commun. Earth Environ.*, 3, 196, doi:10.1038/s43247-
730 022-00536-0, 2022.
- 731 Liu, M., Shen, Y., González-Sampériz, P., Gil-Romera, G., ter Braak, C. J. F., Prentice, I. C.
732 and Harrison, S. P.: Holocene climates of the Iberian Peninsula: pollen-based reconstructions
733 of changes in the west–east gradient of temperature and moisture, *Clim. Past*, 19(4), 803–
734 834, doi:10.5194/cp-19-803-2023, 2023.
- 735 Malmierca-Vallet, I., Sime, L. C. and Members, the D. community: Dansgaard–Oeschger
736 events in climate models: Review and baseline Marine Isotope Stage 3 (MIS3) protocol,
737 *Clim. Past*, 19(5), 915–942, doi:10.5194/cp-19-915-2023, 2023.
- 738 Martrat, B., Grimalt, J. O., Shackleton, N. J., de Abreu, L., Hutterli, M. A. and Stocker, T. F.:
739 Four climate cycles of recurring deep and surface water destabilizations on the Iberian
740 margin, *Science (80-.)*, 317(5837), 502–507, doi:10.1126/science.1139994, 2007.
- 741 Van Meerbeeck, C. J., Renssen, H., Roche, D. M., Wohlfarth, B., Bohncke, S. J. P., Bos, J.
742 A. A., Engels, S., Helmens, K. F., Sánchez-Goñi, M. F., Svensson, A. and Vandenberghe, J.:
743 The nature of MIS 3 stadial–interstadial transitions in Europe: New insights from model–data
744 comparisons, *Quat. Sci. Rev.*, 30(25), 3618–3637, doi:10.1016/j.quascirev.2011.08.002,
745 2011.
- 746 Menviel, L., Timmermann, A., Friedrich, T. and England, M. H.: Hindcasting the continuum
747 of Dansgaard–Oeschger variability: Mechanisms, patterns and timing, *Clim. Past*, 10(1), 63–
748 77, doi:10.5194/cp-10-63-2014, 2014.
- 749 Menviel, L., Skinner, L. C., Tarasov, L. and Tzedakis, P. C.: An ice–climate oscillatory
750 framework for Dansgaard–Oeschger cycles, *Nat. Rev. Earth Environ.*, 1(12), 677–693,
751 doi:10.1038/s43017-020-00106-y, 2020.
- 752 Newnham, R. M., Alloway, B. V, Holt, K. A., Butler, K., Rees, A. B. H., Wilmshurst, J. M.,
753 Dunbar, G. and Hajdas, I.: Last Glacial pollen–climate reconstructions from Northland, New
754 Zealand, *J. Quat. Sci.*, 32(6), 685–703, doi:10.1002/jqs.2955, 2017.
- 755 Peterson, A. T.: Ecological niche conservatism: A time-structured review of evidence, *J.*
756 *Biogeogr.*, 38(5), 817–827, doi:10.1111/j.1365-2699.2010.02456.x, 2011.

- 757 Pini, R., Furlanetto, G., Vallé, F., Badino, F., Wick, L., Anselmetti, F. S., Bertuletti, P., Fusi,
758 N., Morlock, M. A., Delmonte, B., Harrison, S. P., Maggi, V. and Ravazzi, C.: Linking North
759 Atlantic and Alpine Last Glacial Maximum climates via a high-resolution pollen-based
760 subarctic forest steppe record, *Quat. Sci. Rev.*, 294, 107759,
761 doi:10.1016/j.quascirev.2022.107759, 2022.
- 762 Prentice, I. C. and Harrison, S. P.: Ecosystem effects of CO₂ concentration: evidence from
763 past climates, *Clim. Past*, 5(3), 297–307, doi:10.5194/cp-5-297-2009, 2009.
- 764 Prentice, I. C., Cleator, S. F., Huang, Y. H., Harrison, S. P. and Roulstone, I.: Reconstructing
765 ice-age palaeoclimates: Quantifying low-CO₂ effects on plants, *Glob. Planet. Change*, 149,
766 166–176, doi:10.1016/j.gloplacha.2016.12.012, 2017.
- 767 Prentice, I. C., Villegas-Diaz, R. and Harrison, S. P.: Accounting for atmospheric carbon
768 dioxide variations in pollen-based reconstruction of past hydroclimates, *Glob. Planet.*
769 *Change*, 211, 103790, doi:10.1016/j.gloplacha.2022.103790, 2022a.
- 770 Prentice, I. C., Villegas-Diaz, R. and Harrison, S. P.: CO_{dos}: CO₂ correction tools, ,
771 doi:10.5281/zenodo.5083309, 2022b.
- 772 Prud'homme, C., Fischer, P., Jöris, O., Gromov, S., Vinneband, M., Hatté, C., Vonhof, H.,
773 Moine, O., Vött, A. and Fitzsimmons, K. E.: Millennial-timescale quantitative estimates of
774 climate dynamics in central Europe from earthworm calcite granules in loess deposits,
775 *Commun. Earth Environ.*, 3(1), 267, doi:10.1038/s43247-022-00595-3, 2022.
- 776 Qian, H. and Ricklefs, R. E.: Geographical distribution and ecological conservatism of
777 disjunct genera of vascular plants in eastern Asia and eastern North America, *J. Ecol.*, 92(2),
778 253–265, doi:10.1111/j.0022-0477.2004.00868.x, 2004.
- 779 Sánchez-Goñi, M., Cacho, I., Turon, J., Guiot, J., Sierro, F., Peyrouquet, J., Grimalt, J. and
780 Shackleton, N.: Synchronicity between marine and terrestrial responses to millennial scale
781 climatic variability during the last glacial period in the Mediterranean region, *Clim. Dyn.*,
782 19(1), 95–105, doi:10.1007/s00382-001-0212-x, 2002.
- 783 Sánchez-Goñi, M. F., Landais, A., Fletcher, W. J., Naughton, F., Desprat, S. and Duprat, J.:
784 Contrasting impacts of Dansgaard–Oeschger events over a western European latitudinal
785 transect modulated by orbital parameters, *Quat. Sci. Rev.*, 27(11), 1136–1151,

- 786 doi:10.1016/j.quascirev.2008.03.003, 2008.
- 787 Sánchez-Goñi, M. F., Desprat, S., Daniau, A.-L., Bassinot, F. C., Polanco-Martínez, J. M.,
788 Harrison, S. P., Allen, J. R. M., Anderson, R. S., Behling, H., Bonnefille, R., Burjachs, F.,
789 Carrión, J. S., Cheddadi, R., Clark, J. S., Combourieu-Nebout, N., Mustaphi, J. C., Debusk,
790 G. H., Dupont, L. M., Finch, J. M., Fletcher, W. J., Giardini, M., González, C., Gosling, W.
791 D., Grigg, L. D., Grimm, E. C., Hayashi, R., Helmens, K., Heusser, L. E., Hill, T., Hope, G.,
792 Huntley, B., Igarashi, Y., Irino, T., Jacobs, B., Jiménez-Moreno, G., Kawai, S., Kershaw, A.
793 P., Kumon, F., Lawson, I. T., Ledru, M.-P., Lézine, A.-M., Liew, P. M., Magri, D., Marchant,
794 R., Margari, V., Mayle, F. E., McKenzie, G. M., Moss, P., Müller, S., Müller, U. C.,
795 Naughton, F., Newnham, R. M., Oba, T., Pérez-Obiol, R., Pini, R., Ravazzi, C., Roucoux, K.
796 H., Rucina, S. M., Scott, L., Takahara, H., Tzedakis, P. C., Urrego, D. H., van Geel, B.,
797 Valencia, B. G., Vandergoes, M. J., Vincens, A., Whitlock, C. L., Willard, D. A. and
798 Yamamoto, M.: The ACER pollen and charcoal database: a global resource to document
799 vegetation and fire response to abrupt climate changes during the last glacial period, *Earth*
800 *Syst. Sci. Data*, 9(2), 679–695, doi:10.5194/essd-9-679-2017, 2017.
- 801 Sinopoli, G., Peyron, O., Masi, A., Holtvoeth, J., Francke, A., Wagner, B. and Sadori, L.:
802 Pollen-based temperature and precipitation changes in the Ohrid Basin (western Balkans)
803 between 160 and 70 ka, *Clim. Past*, 15(1), 53–71, doi:10.5194/cp-15-53-2019, 2019.
- 804 Stockhecke, M., Timmermann, A., Kipfer, R., Haug, G. H., Kwiecien, O., Friedrich, T.,
805 Menviel, L., Litt, T., Pickarski, N. and Anselmetti, F. S.: Millennial to orbital-scale variations
806 of drought intensity in the Eastern Mediterranean, *Quat. Sci. Rev.*, 133, 77–95,
807 doi:10.1016/j.quascirev.2015.12.016, 2016.
- 808 Timm, O., Timmermann, A., Abe-Ouchi, A., Saito, F. and Segawa, T.: On the definition of
809 seasons in paleoclimate simulations with orbital forcing, *Paleoceanography*, 23(2),
810 doi:10.1029/2007PA001461, 2008.
- 811 Turner, M. G., Wei, D., Prentice, I. C. and Harrison, S. P.: The impact of methodological
812 decisions on climate reconstructions using WA-PLS, *Quat. Res.*, 99, 341–356,
813 doi:10.1017/qua.2020.44, 2020.
- 814 Újvári, G., Bernasconi, S. M., Stevens, T., Kele, S., Páll-Gergely, B., Surányi, G. and
815 Demény, A.: Stadial-interstadial temperature and aridity variations in east central Europe

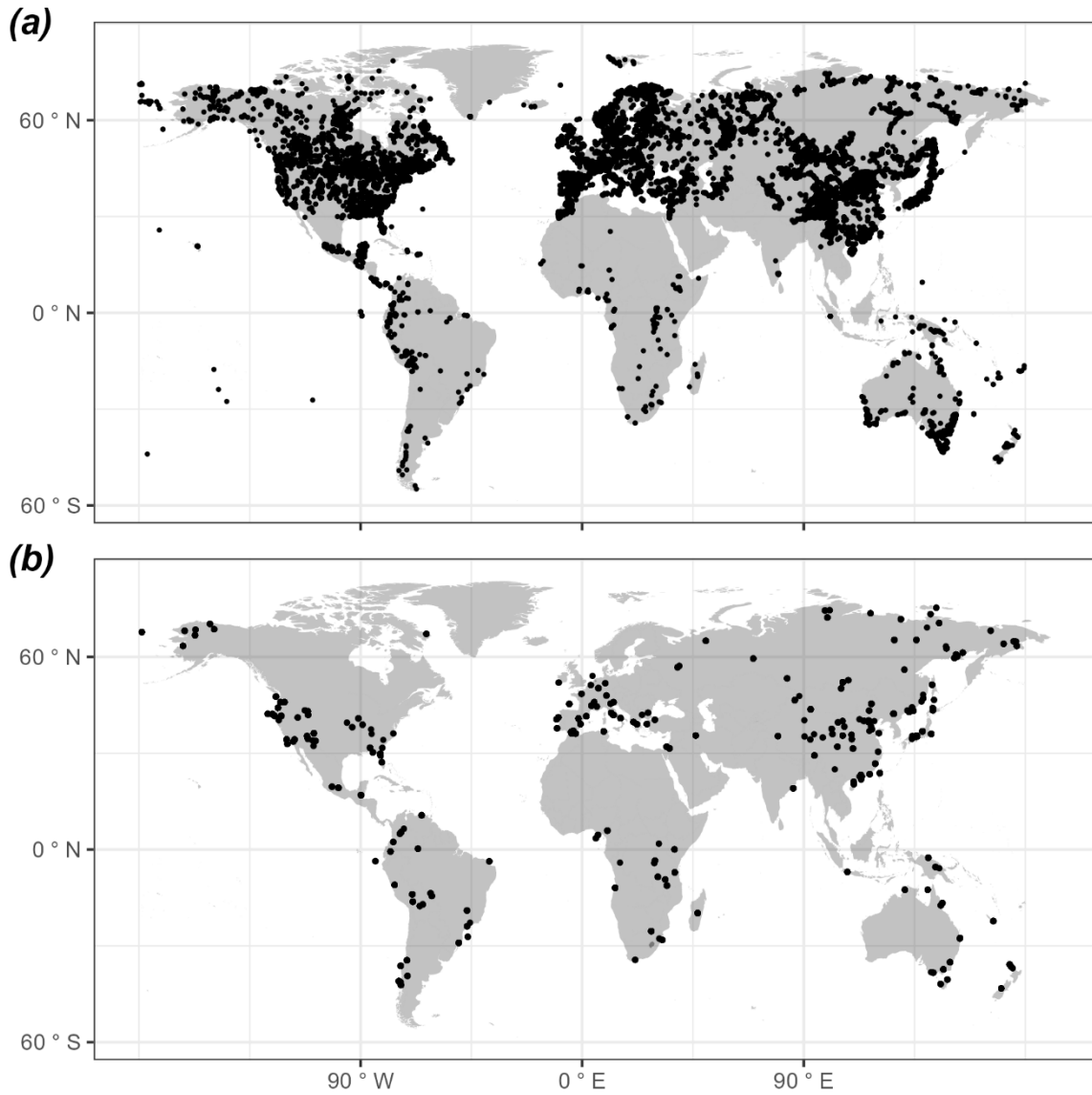
- 816 preceding the Last Glacial Maximum, *Paleoceanogr. Paleoclimatology*, 36(8),
817 e2020PA004170, doi:10.1029/2020PA004170, 2021.
- 818 Veres, D., Bazin, L., Landais, A., Toyé Mahamadou Kele, H., Lemieux-Dudon, B., Parrenin,
819 F., Martinerie, P., Blayo, E., Blunier, T., Capron, E., Chappellaz, J., Rasmussen, S. O.,
820 Severi, M., Svensson, A., Vinther, B. and Wolff, E. W.: The Antarctic ice core chronology
821 (AICC2012): An optimized multi-parameter and multi-site dating approach for the last 120
822 thousand years, *Clim. Past*, 9(4), 1733–1748, doi:10.5194/cp-9-1733-2013, 2013.
- 823 Vettoretti, G. and Peltier, W. R.: Interhemispheric air temperature phase relationships in the
824 nonlinear Dansgaard-Oeschger oscillation, *Geophys. Res. Lett.*, 42(4), 1180–1189,
825 doi:10.1002/2014GL062898, 2015.
- 826 Voelker, A. H. L.: Global distribution of centennial-scale records for Marine Isotope Stage
827 (MIS) 3: a database, *Quat. Sci. Rev.*, 21(10), 1185–1212, doi:10.1016/S0277-3791(01)00139-
828 1, 2002.
- 829 Wang, C., Wang, M., Zhu, S., Wu, X., Yang, S., Yan, Y. and Wen, Y.: Multiple ecological
830 niche modeling reveals niche conservatism and divergence in East Asian Yew (*Taxus*),
831 *Plants*, 14(7), doi:10.3390/plants14071094, 2025.
- 832 Wang, H., Prentice, I. C. and Ni, J.: Data-based modelling and environmental sensitivity of
833 vegetation in China, *Biogeosciences*, 10(9), 5817–5830, doi:10.5194/bg-10-5817-2013, 2013.
- 834 Wang, Y. J., Cheng, H., Edwards, R. L., An, Z. S., Wu, J. Y., Shen, C.-C. and Dorale, J. A.:
835 A high-resolution absolute-dated Late Pleistocene monsoon record from Hulu Cave, China,
836 *Science* (80-.), 294(5550), 2345–2348, doi:10.1126/science.1064618, 2001.
- 837 Warken, S. F., Scholz, D., Spötl, C., Jochum, K. P., Pajón, J. M., Bahr, A. and Mangini, A.:
838 Caribbean hydroclimate and vegetation history across the last glacial period, *Quat. Sci. Rev.*,
839 218, 75–90, doi:10.1016/j.quascirev.2019.06.019, 2019.
- 840 Wei, D., Prentice, I. C. and Harrison, S. P.: The climatic space of European pollen taxa,
841 *Ecology*, 101(8), e03055, doi:10.1002/ecy.3055, 2020.
- 842 Wei, D., González-Sampériz, P., Gil-Romera, G., Harrison, S. P. and Prentice, I. C.: Seasonal
843 temperature and moisture changes in interior semi-arid Spain from the last interglacial to the

- 844 Late Holocene, *Quat. Res.*, 101, 143–155, doi:10.1017/qua.2020.108, 2021.
- 845 Wiens, J. and Graham, C.: Niche conservatism: Integrating evolution, ecology, and
846 conservation biology, *Annu. Rev. Ecol. Evol. Syst.*, 36, 519–539,
847 doi:10.1146/annurev.ecolsys.36.102803.095431, 2005.
- 848 Wiens, J., Ackerly, D., Allen, A., Anacker, B., Buckley, L., Cornell, H., Damschen, E.,
849 Davies, J., Grytnes, J. A., Harrison, S., Hawkins, B., Holt, R., McCain, C. and Stephens, P.:
850 Niche conservatism as an emerging principle in ecology and conservation biology, *Ecol.*
851 *Let.*, 13, 1310–1324, doi:10.1111/j.1461-0248.2010.01515.x, 2010.
- 852 Wolff, E. W., Chappellaz, J., Blunier, T., Rasmussen, S. O. and Svensson, A.: Millennial-
853 scale variability during the last glacial: The ice core record, *Quat. Sci. Rev.*, 29(21), 2828–
854 2838, doi:10.1016/j.quascirev.2009.10.013, 2010.
- 855 Woodward, F. I.: *Climate and Plant Distribution*, Cambridge University Press, Cambridge,
856 UK., 1987.
- 857 Wu, H., Guiot, J., Brewer, S. and Guo, Z.: Climatic changes in Eurasia and Africa at the last
858 glacial maximum and mid-Holocene: Reconstruction from pollen data using inverse
859 vegetation modelling, *Clim. Dyn.*, 29(2), 211–229, doi:10.1007/s00382-007-0231-3, 2007.
- 860 Yin, X., Jarvie, S., Guo, W.-Y., Deng, T., Mao, L., Zhang, M., Chu, C., Qian, H., Svenning,
861 J.-C. and He, F.: Niche overlap and divergence times support niche conservatism in eastern
862 Asia–eastern North America disjunct plants, *Glob. Ecol. Biogeogr.*, 30(10), 1990–2003,
863 doi:10.1111/geb.13360, 2021.
- 864 Zander, P. D., Böhl, D., Sirocko, F., Auderset, A., Haug, G. H. and Martínez-García, A.:
865 Reconstruction of warm-season temperatures in central Europe during the past 60 000 years
866 from lacustrine branched glycerol dialkyl glycerol tetraethers (brGDGTs), *Clim. Past*, 20(4),
867 841–864, doi:10.5194/cp-20-841-2024, 2024.
- 868 Zhou, B.-R., Liao, M.-N., Li, K., Xu, D.-Y., Chen, H.-Y., Ni, J., Cao, X.-Y., Kong, Z.-C.,
869 Xu, Q.-H., Zhang, Y., Herzsich, U., Cai, Y.-L., Chen, B.-S., Chen, J.-A., Chen, L.-K.,
870 Cheng, B., Gao, Y., Huang, X.-Z., Li, S.-F., Li, W.-Y., Liu, K.-B., Liu, G.-X., Liu, P.-M.,
871 Liu, X.-Q., Ma, C.-M., Song, C.-Q., Sun, X.-J., Tang, L.-Y., Wang, M.-H., Wang, Y.-B., Xu,
872 J.-S., Yan, S., Yang, X.-D., Yao, Y.-F., Ye, C.-Y., Zhang, Z.-Y., Zhao, Z.-Y., Zheng, Z. and

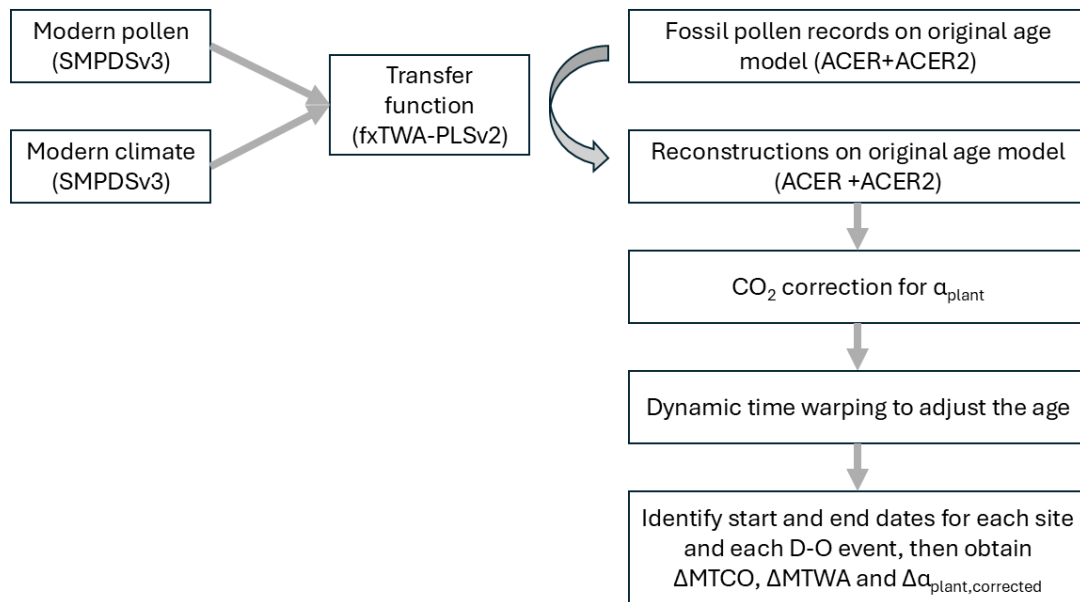
- 873 Zhu, C.: A fossil pollen dataset of China, *Chinese J. Plant Ecol.*, 47(10), 1453–1463 [online]
874 Available from: <https://www.plant-ecology.com>, 2023.
- 875 Zorzi, C., Desprat, S., Clément, C., Thirumalai, K., Oliviera, D., Anupama, K., Prasad, S. and
876 Martinez, P.: When eastern India oscillated between desert versus savannah-dominated
877 vegetation, *Geophys. Res. Lett.*, 49(16), e2022GL099417, doi:10.1029/2022GL099417,
878 2022.
- 879 Zumaque, J., de Vernal, A., Fréchette, B., Guiot, J., Sánchez-Goñi, M. F., Barhoumi, C.,
880 Peyron, O., Peros, M., Burke, A., Camuera, J., Jiménez-Moreno, G. and Ramos-Román, M.
881 J.: Decoupled winter and summer climate changes in southern Europe during the Dansgaard-
882 Oeschger cycles, *Quat. Sci. Rev.*, 359, 109273, doi:10.1016/j.quascirev.2025.109273, 2025.
- 883

884 **Figures and Tables**

885 Figure 1: Map showing the locations of (a) modern pollen records used to derive the pollen-
886 climate transfer functions, and (b) fossil pollen records covering the interval 50-30 ka used for
887 the climate reconstructions.



890 Figure 2: Flow chart showing the methodology.



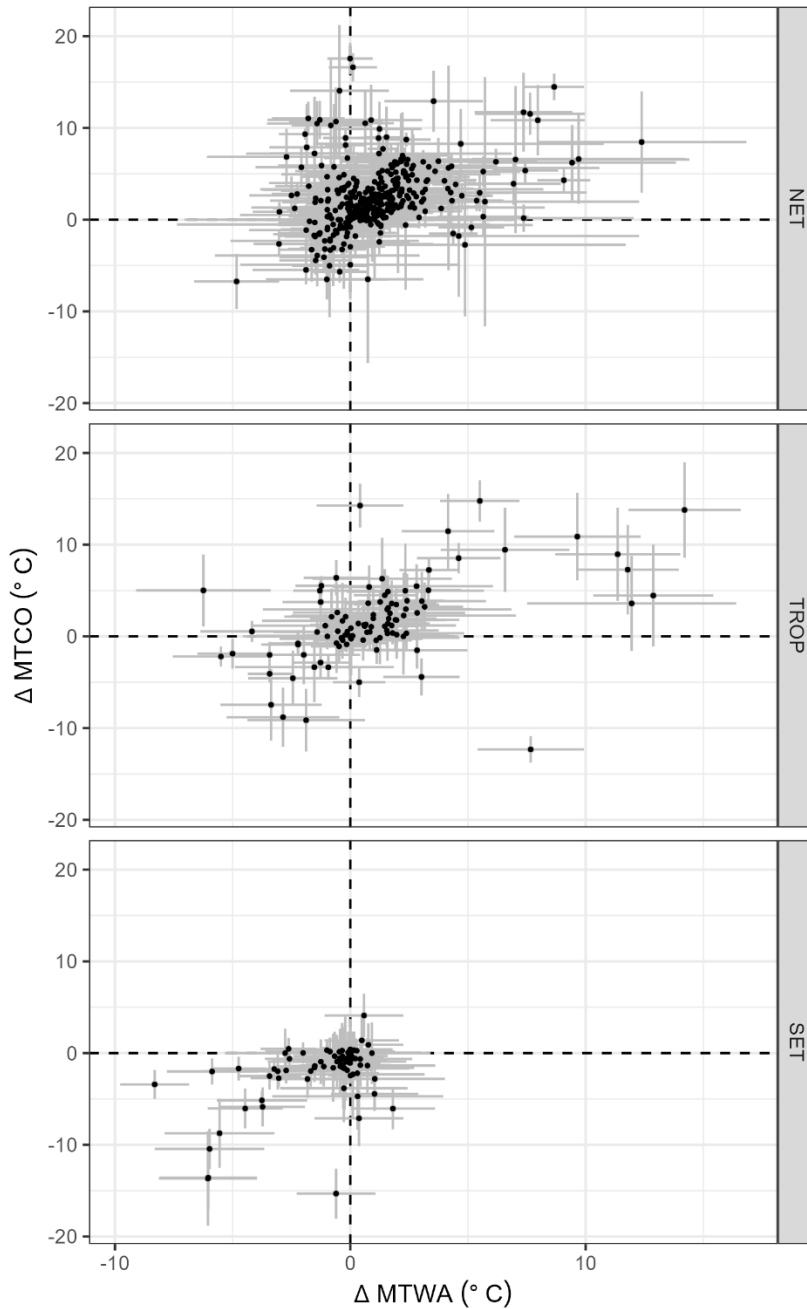
891

892

893

894

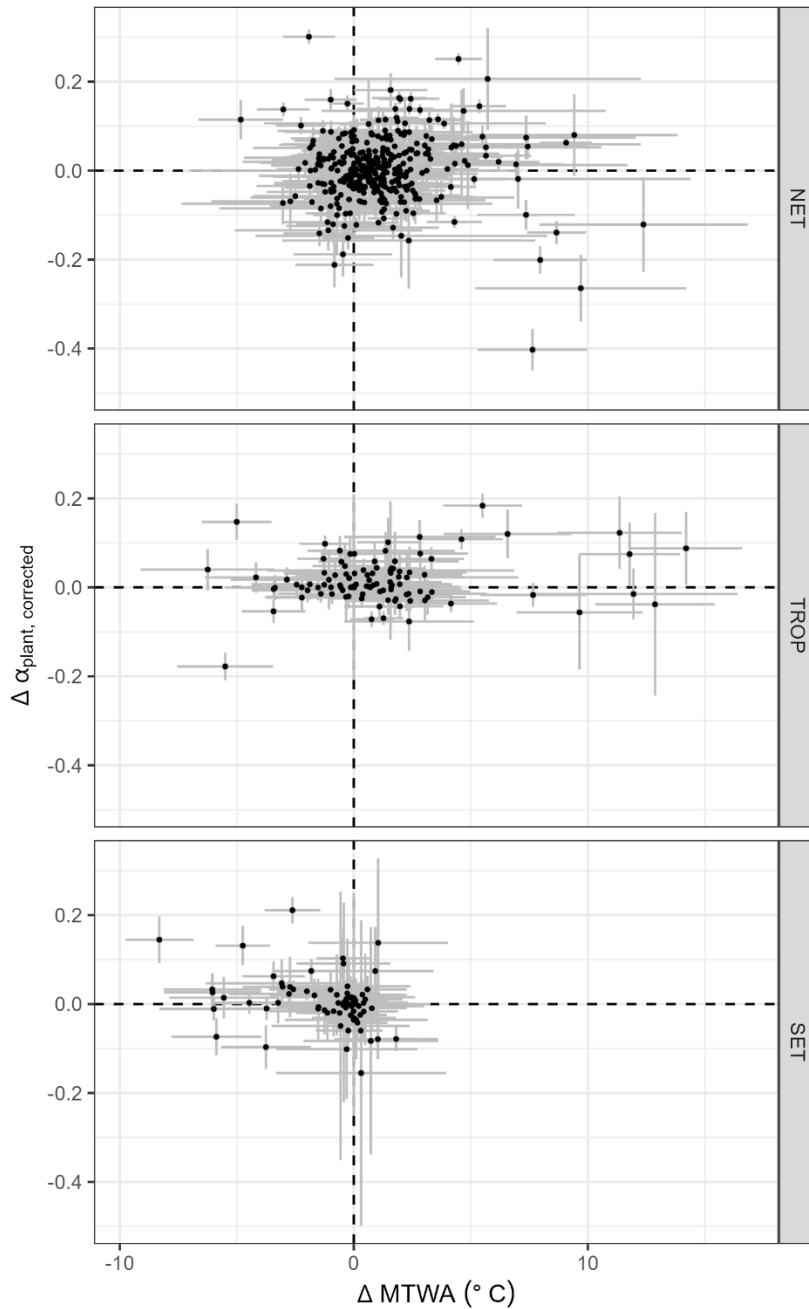
895 Figure 3: Scatter plot of the change in mean temperature of the coldest month (ΔMTCO) versus
896 the change in mean temperature of the warmest month (ΔMTWA) during individual
897 Dansgaard-Oeschger (D-O) events at individual sites. The points are grouped into the northern
898 extratropics (NET, north of 23.5°N), the tropics (TROP, between 23.5°N and 23.5°S) and the
899 southern extratropics (SET, south of 23.5°S). The grey lines indicate ± 1 error of the change.



900

901

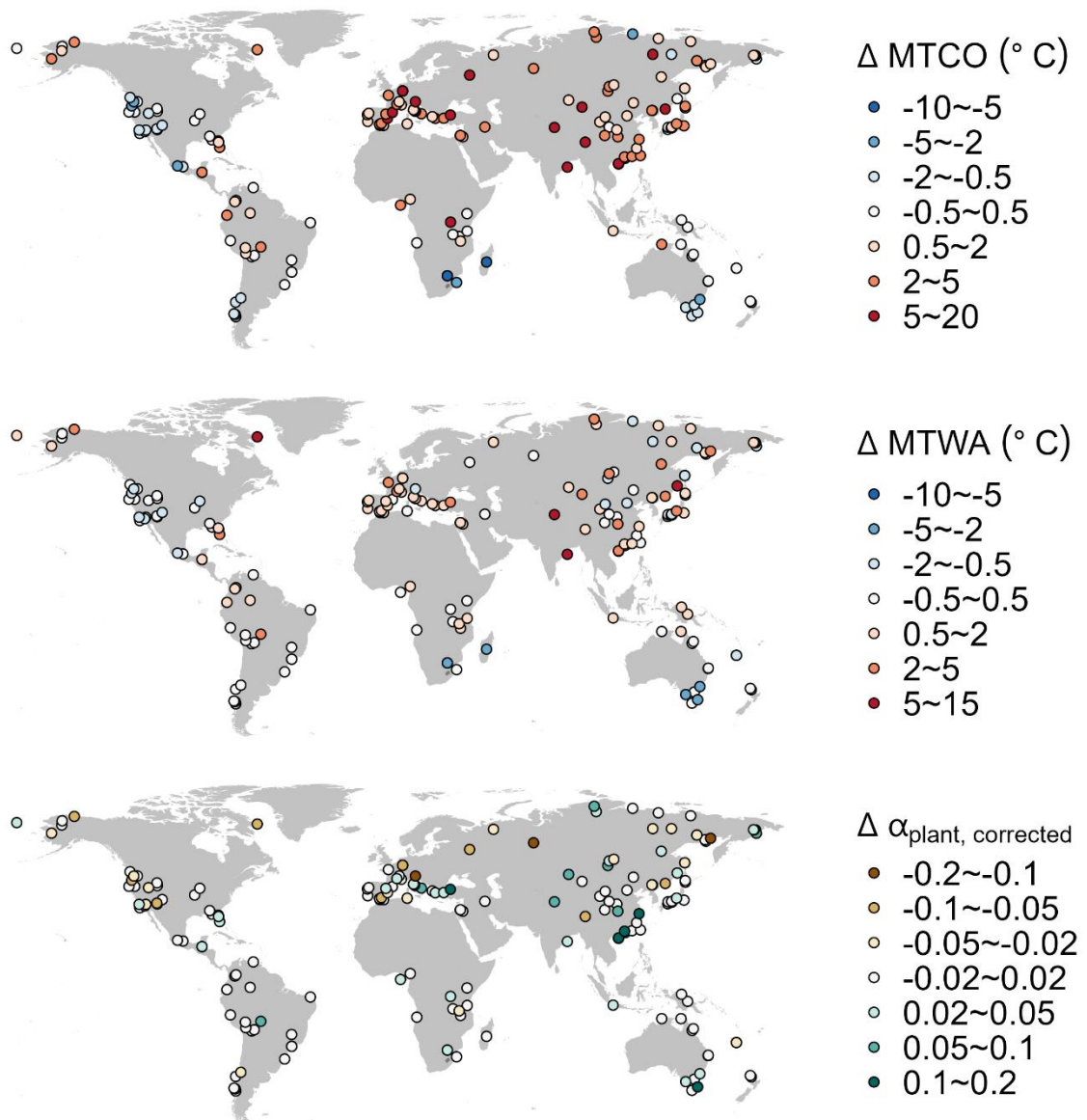
902 Figure 4: Scatter plot of the change in CO₂-corrected plant-available moisture ($\Delta\alpha_{\text{plant,corrected}}$)
903 versus the change in mean temperature of the warmest month (ΔMTWA) during individual
904 Dansgaard-Oeschger (D-O) events at individual sites. The points are grouped into the northern
905 extratropics (NET, north of 23.5°N), the tropics (TROP, between 23.5°N and 23.5°S) and the
906 southern extratropics (SET, south of 23.5°S). The grey lines indicate ± 1 error of the change.



907

908

909 Figure 5: Map showing the median change of site-based reconstructions for Dansgaard-
 910 Oeschger (D-O) events 5 to 12. The panels from top to bottom show the changes in mean
 911 temperature of the coldest month (ΔMTCO), mean temperature of the warmest month
 912 (ΔMTWA) and CO_2 -corrected plant-available moisture ($\Delta\alpha_{\text{plant,corrected}}$).

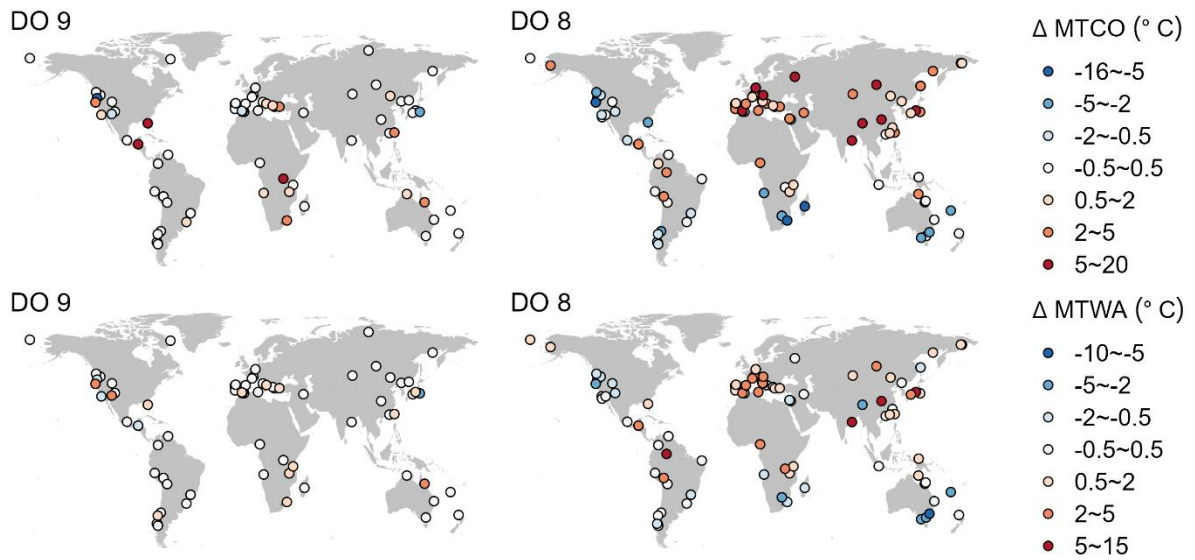


913

914

915

916 Figure 6: Map showing the change in mean temperature of the coldest month (ΔMTCO) and
 917 the change in mean temperature of the warmest month (ΔMTWA) for D-O 9 (a weak event)
 918 and D-O 8 (a strong event). The upper panel shows ΔMTCO , while the lower panel shows
 919 ΔMTWA .

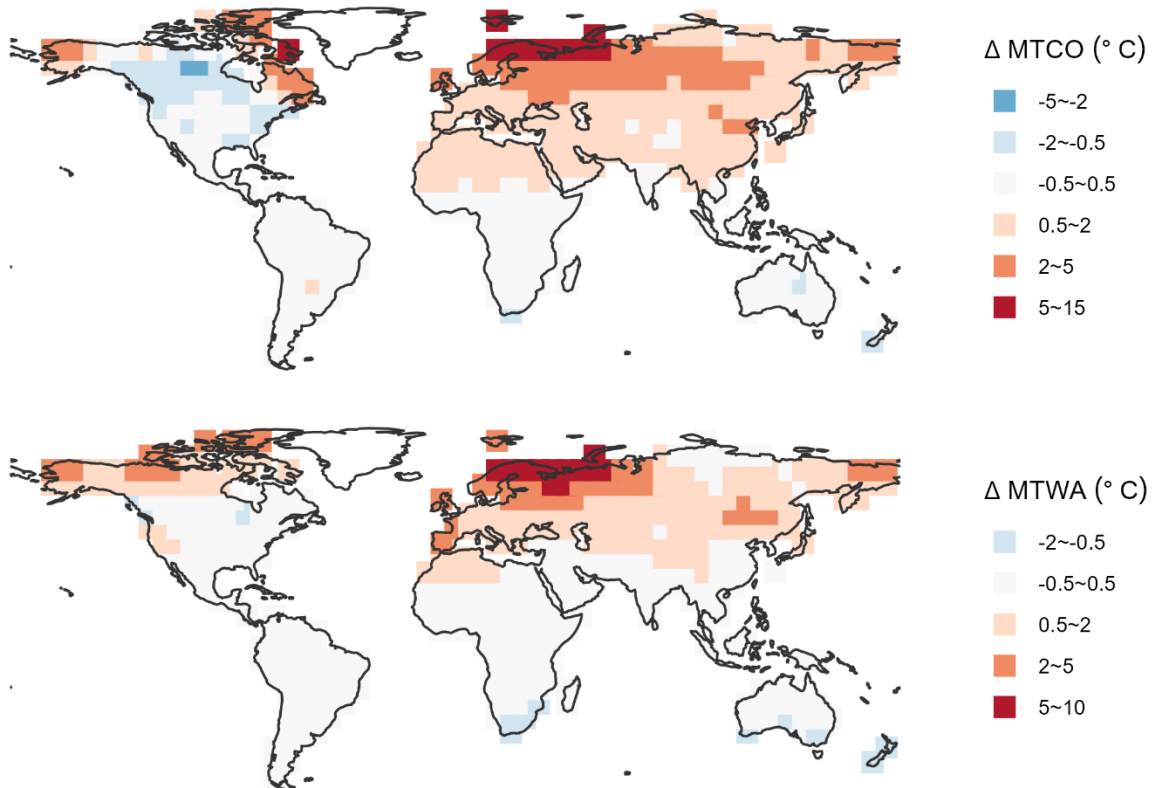


920

921

922

923 Figure 7: Map showing the median change of LOVECLIM simulations over (ice-free) land for
924 Dansgaard-Oeschger (D-O) events 5 to 12. The upper panel shows the change in mean
925 temperature of the coldest month (ΔMTCO), and the lower panel shows the change in mean
926 temperature of the warmest month (ΔMTWA).

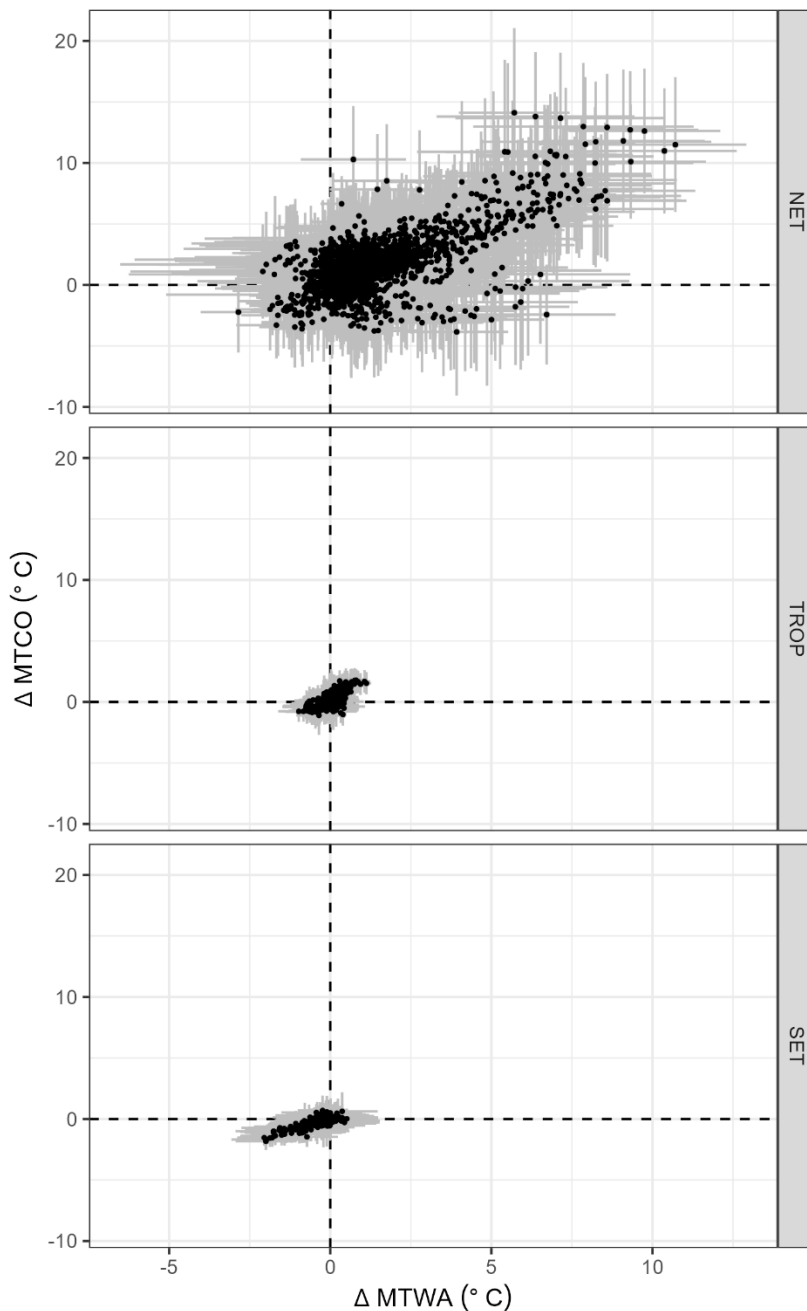


927

928

929

930 Figure 8: Scatter plot of the change in mean temperature of the coldest month (ΔMTCO) versus
931 the change in mean temperature of the warmest month (ΔMTWA) during individual
932 Dansgaard-Oeschger (D-O) events at individual (ice-free) land grids simulated by the
933 LOVECLIM model, using the same way to identify changes as the reconstructions. The points
934 are grouped into the northern extratropics (NET, north of 23.5°N), the tropics (TROP, between
935 23.5°N and 23.5°S) and the southern extratropics (SET, south of 23.5°S). The grey lines
936 indicate ± 1 error of the change.



937

938

939 Table 1: Site information of the fossil pollen records covering the interval 50-30 ka. The
 940 references with full citation are given in Supplementary Materials, section 3. lat is the latitude,
 941 lon is the longitude, elv is the elevation (unit: m). TERR means terrestrial record, MARI means
 942 marine record. n_{due} is the number of D-O events that should be found based on the time interval
 943 covered by the record. n_{miss} is the number of D-O events that were not identified. n_{low} is the
 944 number of D-O events missed because of low resolution of that part of the record. Some
 945 sites provide records in 50-30 ka but do not cover the intervals of the D-O events; some marine
 946 sites are too far from the land to extract GWR modern MTGR to apply CO₂ correction; these
 947 sites are all indicated by NA in n_{due} , n_{miss} and n_{low} .

name	lat	lon	elv	type	source	n_{due}	n_{miss}	n_{low}
Abric Romani	41.53	1.68	350	TERR	ACER	2	0	0
Akulinin Exposure P1282	47.12	138.55	20	TERR	Legacy2	1	0	0
Alut Lake	60.14	152.31	480	TERR	Cao et al. (2019, 2020)	7	1	1
Anderson Pond (ANDERSON)	36.03	-85.50	303	TERR	Legacy2	NA	NA	NA
Auel_AU2	50.28	6.59	457	TERR	AUTHOR	7	0	0
Aueler Maar ELSA AU3	50.28	6.60	456	TERR	Pangaea	3	0	0
Aueler Maar ELSA AU4	50.28	6.59	457	TERR	Pangaea	7	2	2
Azzano Decimo	45.88	12.72	10	TERR	ACER	4	0	0
Bajondillo	36.62	-4.50	20	TERR	Legacy2	2	0	0
Baldwin Lake	34.28	-116.81	2060	TERR	Legacy2	4	1	1
Balikun Lake	43.68	92.80	1575	TERR	Legacy2	NA	NA	NA
Balikun Lake BLK11A	43.68	92.80	1575	TERR	AUTHOR	2	0	0
Bambili 2	5.93	10.24	2323	TERR	Legacy2	5	1	1
Bandung DPDR-II	-6.99	107.73	662	TERR	Legacy2	4	2	2
Bay of Biscay	45.35	-5.22	-4100	MARI	Legacy2	NA	NA	NA
Bear Lake (BL00-1E)	41.95	-111.31	1805	TERR	ACER	7	2	2
Bereyekh River	63.28	147.75	800	TERR	Cao et al. (2019, 2020)	NA	NA	NA
Biggsville [Cessford Quarry]	40.86	-90.88	198	TERR	Legacy2	1	0	0
Bolotnyii Stream Exposure 117	42.85	132.78	4	TERR	Legacy2	2	1	1
Bolshoe Toko PG2133	56.04	130.87	903	TERR	Legacy2	2	0	0
Bolshoy Lyakhovsky Island	73.33	141.50	7	TERR	Legacy2	NA	NA	NA
Boney Spring	38.11	-93.37	210	TERR	Legacy2	1	1	1

Byllatskoye Exposure, Byllat River, Indigirka Basin	69.17	140.06	316	TERR	Legacy2	NA	NA	NA
Cala Conto	-17.57	-65.93	2700	TERR	Legacy2	2	2	2
Caledonia Fen	-37.33	146.73	1280	TERR	ACER	7	2	2
Cambara do Sul	-29.05	-50.10	1040	TERR	ACER	7	2	0
Camel Lake	30.26	-85.01	20	TERR	ACER	2	1	1
Carp Lake	45.91	-120.88	720	TERR	ACER	8	3	3
Changping CHZK1	40.18	116.22	49	TERR	Zhou et al. (2023)	NA	NA	NA
Chenghai CH2	23.48	116.80	5	TERR	Zhou et al. (2023)	4	1	1
Cheremushka Bog	52.75	108.08	1500	TERR	Cao et al. (2019, 2020)	1	0	0
Colonia	-23.87	-46.71	900	TERR	ACER	7	5	5
Colonia CO3	-23.87	-46.71	900	TERR	Legacy2	7	4	4
Core Trident 163 31B	-3.61	-83.96	-3210	MARI	ACER	NA	NA	NA
Correo	44.56	6.00	1100	TERR	Legacy2	1	0	0
Crystal Lagoon	-40.48	148.35	8	TERR	Legacy2	1	0	0
Daihai Lake-Wajianggou	40.58	112.67	1500	TERR	Zhou et al. (2023)	NA	NA	NA
Dajiu Lake DJH-1	31.49	110.00	1751	TERR	Zhou et al. (2023)	8	1	1
Dalai Nur Lake-Haiyan	43.28	116.58	1200	TERR	Zhou et al. (2023)	NA	NA	NA
Daluoba	47.83	88.20	2020	TERR	Zhou et al. (2023)	NA	NA	NA
Dar Fatma	36.82	8.77	780	TERR	Legacy2	7	2	2
Daxing DZK1	39.72	116.32	49	TERR	Zhou et al. (2023)	NA	NA	NA
Dead Sea	31.51	35.47	-428	TERR	Pangaea	6	0	0
Demyanskoye	59.50	69.50	65	TERR	Cao et al. (2019, 2020)	1	0	0
Deva-Deva	-7.12	37.62	2600	TERR	Legacy2	4	1	1
Diexi Lake	32.04	103.68	2334	TERR	Zhou et al. (2023)	2	0	0
Dikikh Olyenyeyi Lake	67.75	-178.83	300	TERR	Cao et al. (2019, 2020)	3	1	1
Eastern Niger Delta	4.55	6.43	0	TERR	Legacy2	NA	NA	NA
Elikchan 4 Lake	60.75	151.88	810	TERR	Cao et al. (2019, 2020)	3	1	1
Emanda	65.29	135.76	671	TERR	Legacy2	4	1	1
Enmynveem River (mammoth site)	68.17	165.93	400	TERR	Legacy2	NA	NA	NA
Enmynveem River1	68.17	165.93	400	TERR	Cao et al. (2019, 2020)	NA	NA	NA

Erlongwan Maar Lake	42.30	126.37	724	TERR	Zhou et al. (2023)	2	0	0
Ershilipu	36.93	116.65	50	TERR	Zhou et al. (2023)	NA	NA	NA
EW9504-17 PC	42.23	-125.81	-2671	MARI	ACER	NA	NA	NA
F2-92-P29	32.90	-119.73	-1475	MARI	ACER	2	2	2
Faddeyevskiy	75.33	143.83	30	TERR	Legacy2	NA	NA	NA
Fargher Lake	45.88	-122.58	200	TERR	ACER	8	2	1
Feng Suancigou Feng	35.51	105.81	1840	TERR	Zhou et al. (2023)	1	1	1
Fog Lake	67.18	-63.25	422	TERR	Legacy2	2	1	1
Fundo Nueva	-41.28	-73.83	66	TERR	ACER	5	1	0
Fuquene	5.45	-73.46	2540	TERR	ACER	7	3	3
Furamoos	47.98	9.88	662	TERR	ACER	NA	NA	NA
Gantang SZY	26.77	119.03	1007	TERR	Zhou et al. (2023)	5	1	1
GeoB2107-3	-27.18	-46.45	-1048	MARI	Legacy2	NA	NA	NA
GeoB3104	-3.67	-37.72	-767	MARI	ACER	1	1	1
Girraween Lagoon	-12.52	131.08	25	TERR	AUTHOR	5	1	1
Goshen Springs	31.72	-86.13	105	TERR	Legacy2	2	2	2
Grass Lake	41.65	-122.17	1537	TERR	Legacy2	3	0	0
Grays Lake (GRAYSG1)	43.07	-111.44	1195	TERR	Legacy2	4	1	1
Grays Lake (GRAYSG6)	43.07	-111.44	1195	TERR	Legacy2	NA	NA	NA
Guangzhou GZ-2	22.71	113.51	1	TERR	Zhou et al. (2023)	3	2	2
Guangzhou GZ-4	23.27	113.21	4	TERR	Zhou et al. (2023)	1	0	0
Gytgykai Lake	63.42	176.57	102	TERR	Cao et al. (2019, 2020)	1	0	0
Hachihama	34.55	133.95	6	TERR	Legacy2	3	1	1
Hangzhou HQB7	30.47	120.21	2	TERR	Zhou et al. (2023)	1	0	0
Hay Lake	34.00	-109.43	2780	TERR	ACER	NA	NA	NA
Headwaters Opasnaya River	48.23	138.48	1320	TERR	Legacy2	NA	NA	NA
Hosoike Moor	35.35	134.13	970	TERR	Legacy2	4	2	2
Huguangyan Maar Lake B	21.15	110.28	88	TERR	Zhou et al. (2023)	NA	NA	NA
Huinamarca (Lake Titicaca)	-16.23	-68.77	3810	TERR	ACER	3	0	0
Indigirka lowlands	70.58	145.00	20	TERR	Cao et al. (2019, 2020)	1	0	0
Ioannina	39.75	20.85	470	TERR	ACER	8	1	0
IODP Site 353-U1446A	19.08	85.73	-1430	MARI	Pangaea	6	1	1
Iwaya site	35.52	135.89	20	TERR	Legacy2	3	1	1

Jackson Pond (JACKSN07)	37.43	-85.72	260	TERR	Legacy2	NA	NA	NA
Jiangcun	34.40	109.50	650	TERR	Zhou et al. (2023)	3	0	0
Joe Lake	66.77	-157.22	183	TERR	ACER	3	1	1
Julietta Lake	61.34	154.56	880	TERR	Cao et al. (2019, 2020)	3	0	0
Kai Iwa	-35.82	173.65	70	TERR	AUTHOR	6	2	2
Kaiyak Lake	68.14	-161.44	190	TERR	Legacy2	NA	NA	NA
Kalaloch	47.63	-124.38	24	TERR	Legacy2	8	1	0
Kalistratikha	53.33	83.25	190	TERR	Cao et al. (2019, 2020)	NA	NA	NA
Kalistratikha Exposure	53.33	83.25	190	TERR	Legacy2	NA	NA	NA
Kamiyoshi Basin (KY01)	35.10	135.59	335	TERR	ACER	1	0	0
Kashiru Bog	-3.47	29.57	2240	TERR	ACER	NA	NA	NA
Kenbuchi Basin	44.05	142.38	135	TERR	ACER	3	0	0
Khoe	51.34	142.14	15	TERR	ACER	1	0	0
Khoe, Sakhalin Island	51.34	142.14	15	TERR	Cao et al. (2019, 2020)	4	2	2
Kirgirlakh Stream, Berelyekh River Basin (DIMA2)	62.67	147.98	700	TERR	Legacy2	NA	NA	NA
Kirgirlakh Stream, Berelyekh River Basin (DIMA3)	62.67	147.98	700	TERR	Legacy2	1	0	0
Kirgirlakh Stream_2	62.67	147.98	700	TERR	Cao et al. (2019, 2020)	1	1	1
Kohuora	-36.95	174.87	5	TERR	ACER	NA	NA	NA
Komanimambuno Mire	-5.82	145.09	2740	TERR	Legacy2	NA	NA	NA
Kunming Basin KZ2-3	25.00	102.62	1890	TERR	Zhou et al. (2023)	NA	NA	NA
Kupena (KUPENA3)	41.98	24.33	1356	TERR	Legacy2	NA	NA	NA
Kurota Lowland	35.52	135.88	20	TERR	ACER	1	0	0
KW31	3.52	5.57	-1181	MARI	ACER	1	0	0
La Laguna	4.92	-74.03	2900	TERR	ACER	1	0	0
Labaz lake (LAO6-95)	72.29	99.61	42	TERR	Legacy2	2	1	0
Lac du Bouchet - DIGI	44.83	3.82	1200	TERR	ACER	8	1	0
Lac Emeric	-22.30	166.97	230	TERR	Legacy2	3	1	1
Lac Suprin	-22.29	166.99	235	TERR	Legacy2	4	2	2
Lagaccione	42.57	11.80	355	TERR	ACER	3	0	0
Lago Grande di Monticchio	40.94	15.61	656	TERR	ACER	8	0	0
Lagoa Campestre de Salitre (SALILC3)	-19.00	-46.77	980	TERR	Legacy2	3	2	2
Lagoa das Patas	0.27	-66.68	300	TERR	Legacy2	4	1	1

Laguna Bella Vista	-13.62	-61.55	600	TERR	ACER	2	1	1
Laguna Chaplin	-14.47	-61.07	600	TERR	ACER	NA	NA	NA
Laguna Ciega	6.48	-72.39	3510	TERR	Legacy2	NA	NA	NA
Laguna Junin	-11.00	-76.17	4100	TERR	Legacy2	5	2	2
Lake Ailike	46.54	86.36	278	TERR	AUTHOR	5	0	0
Lake Albert (Lake Mobutu Sese Seko)	1.83	31.17	619	TERR	Legacy2	NA	NA	NA
Lake Annie	27.21	-81.35	34	TERR	Legacy2	1	0	0
Lake Baikal_BDP99	52.09	105.84	456	TERR	Pangaea	7	0	0
Lake Billyakh	65.28	126.78	340	TERR	ACER	3	0	0
Lake Biwa (BIW95-4)	35.25	136.05	84	TERR	ACER	3	0	0
Lake Carpentaria	-12.52	140.35	-60	MARI	Legacy2	4	2	2
Lake Chalco CHA08	19.25	-98.97	2250	TERR	AUTHOR	5	1	1
Lake Consuelo (CON1)	-13.95	-68.99	1360	TERR	ACER	7	2	2
Lake E5	68.64	-149.46	803	TERR	Legacy2	NA	NA	NA
Lake Elsinore	33.66	-117.35	376	TERR	Legacy2	1	0	0
Lake Fimon	45.47	11.53	23	TERR	AUTHOR	NA	NA	NA
Lake George	-35.09	149.43	673	TERR	Legacy2	4	0	0
Lake Hordorli	-2.54	140.59	798	TERR	Legacy2	4	0	0
Lake Iznik	40.43	29.53	88	TERR	Legacy2	1	0	0
Lake Malawi	-11.22	34.42	470	TERR	ACER	5	2	2
Lake Masoko	-9.33	33.75	840	TERR	ACER	2	1	1
Lake Nero (NERO2)	57.18	39.45	93	TERR	Legacy2	NA	NA	NA
Lake Nojiri	36.83	138.22	657	TERR	ACER	8	0	0
Lake Patzcuaro	19.58	-101.58	2044	TERR	Legacy2	2	1	1
Lake Peten-Itza	16.99	-89.82	110	TERR	Legacy2	8	1	1
Lake Quexil	16.92	-89.82	110	TERR	Legacy2	4	2	2
Lake Selina	-41.88	145.61	516	TERR	Legacy2	1	0	0
Lake Tanganyika (KH3)	-8.50	30.75	773	TERR	Legacy2	4	2	2
Lake Tanganyika (KH4)	-8.50	30.75	773	TERR	Legacy2	NA	NA	NA
Lake Tanganyika [north basin] (SD24TAN)	-4.19	29.31	773	TERR	Legacy2	NA	NA	NA
Lake Tritrivakely	-19.78	46.92	1778	TERR	Legacy2	5	1	0
Lake Tulane	29.83	-81.95	36	TERR	ACER	7	1	1
Lake Wangoom LW87 core	-38.35	142.60	100	TERR	ACER	4	0	0
Lake Xinias	39.05	22.27	500	TERR	ACER	8	3	3
Lake Yamozero	65.02	50.23	213	TERR	Legacy2	2	0	0
Lake Zeribar	35.53	46.12	1288	TERR	Legacy2	7	1	1
Ledovyi Obryv Exposure, Northern Section	64.10	171.18	57	TERR	Legacy2	NA	NA	NA
Les Echets G - DIGI	45.90	4.93	267	TERR	ACER	8	0	0
Levantine Basin	32.03	34.28	0	TERR	Legacy2	4	1	1

Levinson Lessing Lake PG1228	74.47	98.64	47	TERR	Cao et al. (2019, 2020)	1	0	0
Little Lake	44.16	-123.58	217	TERR	ACER	5	0	0
Lop Nur K1	40.28	90.25	780	TERR	Zhou et al. (2023)	NA	NA	NA
Luanhaizi Lake LH2	37.59	101.35	3200	TERR	Zhou et al. (2023)	1	0	0
Luochuan	35.75	109.42	1068	TERR	Zhou et al. (2023)	NA	NA	NA
Lynchs Crater	-17.37	145.70	760	TERR	ACER	7	4	4
Malyi Krechet Lake	64.80	175.53	32	TERR	Legacy2	2	0	0
Mamontovy Khayata	71.77	129.45	0	TERR	Cao et al. (2019, 2020)	3	0	0
Mamontovy Klyk	73.61	117.13	25	TERR	Legacy2	1	0	0
MD01-2421	36.02	141.77	-2224	MARI	ACER	8	1	0
MD03-2622 Cariaco Basin	10.71	-65.17	-877	MARI	ACER	7	5	3
MD04-2845	45.35	-5.22	-4100	MARI	ACER	NA	NA	NA
MD84-629	32.07	34.35	-745	MARI	ACER	5	1	1
MD95-2039	40.58	-10.35	-3381	MARI	ACER	8	1	1
MD95-2042	37.80	-10.17	-3148	MARI	ACER	8	1	1
MD95-2043	36.14	-2.62	-1841	MARI	ACER	8	1	1
MD99-2331	41.15	-9.68	-2110	MARI	ACER	7	1	1
Megali Limni	39.10	26.32	323	TERR	ACER	6	0	0
Melkoye Lake	64.86	175.23	36	TERR	Cao et al. (2019, 2020)	1	0	0
Mereya River	46.62	142.92	4	TERR	Cao et al. (2019, 2020)	NA	NA	NA
Mfabeni Peatland	-28.15	32.52	11	TERR	ACER	4	1	0
Middle Butte Cave	43.37	-112.62	1590	TERR	Legacy2	NA	NA	NA
Milin	29.31	94.35	2982	TERR	Zhou et al. (2023)	3	0	0
Moershoofd	51.25	3.52	2	TERR	Legacy2	NA	NA	NA
Morro de Itapeva	-22.78	-45.53	1850	TERR	Legacy2	NA	NA	NA
Mud Lake (MUDLAKE)	29.30	-81.87	9	TERR	Legacy2	4	1	1
Muscotah Marsh	39.53	-95.51	280	TERR	Legacy2	NA	NA	NA
Nachtigall	51.81	9.40	95	TERR	Legacy2	NA	NA	NA
Nakafurano	43.37	142.43	173	TERR	ACER	2	1	1
Native Companion Lagoon	-27.68	153.41	20	TERR	ACER	4	2	2
Navarres	39.10	-0.68	225	TERR	ACER	3	0	0
Ngamakala Pound (GAMA4)	-4.08	15.38	400	TERR	Legacy2	NA	NA	NA
Ngoring Lake CK6	34.92	97.73	4272	TERR	Zhou et al. (2023)	NA	NA	NA

Noordzee T121	54.10	4.21	0	TERR	Legacy2	NA	NA	NA
Northern Coast of Onemen Gulf	64.78	176.17	18	TERR	Legacy2	3	0	0
ODP 1233 C	-41.00	-74.45	-838	MARI	ACER	8	2	1
ODP 1234	-36.22	-73.68	-1015	MARI	ACER	8	0	0
ODP 820	-16.63	146.30	-280	MARI	ACER	5	3	3
ODP site 976	36.20	-4.30	-1108	MARI	ACER	8	1	0
ODP1019	41.66	-124.91	989	MARI	ACER	7	3	3
ODP1078C	-11.92	13.40	-426	MARI	ACER	8	2	1
ODP893A	34.28	-120.03	-577	MARI	ACER	8	0	0
Oil Lake	70.29	-151.17	745	TERR	Legacy2	2	0	0
Okarito Pakihi	-43.24	170.22	70	TERR	ACER	NA	NA	NA
Ovrazhnyi Stream-2	43.25	134.57	10	TERR	Cao et al. (2019, 2020)	NA	NA	NA
Ovrazhnyii-1 Stream Exposure	43.25	134.57	8	TERR	Legacy2	NA	NA	NA
Ovrazhnyii-2 Exposure 667-842	43.25	134.57	10	TERR	Legacy2	NA	NA	NA
Padul	37.01	-3.60	726	TERR	AUTHOR	6	2	2
Paramonovskii Stream	43.20	133.75	120	TERR	Cao et al. (2019, 2020)	NA	NA	NA
Paramonovskii Stream Exposure 4980	43.20	133.75	120	TERR	Legacy2	NA	NA	NA
Pavlovka Exposure 988	44.32	134.00	300	TERR	Legacy2	NA	NA	NA
Peloncillo Mountains	32.29	-109.09	1400	TERR	Legacy2	NA	NA	NA
Peschanka Exposure 155	43.30	132.12	12	TERR	Legacy2	NA	NA	NA
Pittsburg Basin	38.90	-89.19	162	TERR	Legacy2	NA	NA	NA
Pleshevo Lake	56.77	38.78	148	TERR	Legacy2	2	0	0
Potato Lake	34.45	-111.33	2222	TERR	ACER	1	1	1
Poutu	-36.38	174.13	82	TERR	AUTHOR	1	1	1
Pretoria Saltpan	-25.41	28.08	1150	TERR	Legacy2	4	0	0
Qingdao ZK2	36.29	120.46	31	TERR	Zhou et al. (2023)	NA	NA	NA
Qingdao ZK3	36.26	120.64	7	TERR	Zhou et al. (2023)	NA	NA	NA
Rahue	-39.37	-70.93	1000	TERR	Legacy2	NA	NA	NA
Reenadinna Wood	52.01	-9.53	20	TERR	Legacy2	NA	NA	NA
Rice Lake (Rice Lake 81)	40.30	-123.22	1100	TERR	ACER	NA	NA	NA
Rietvlei-Still Bay	-34.35	21.54	17	TERR	Legacy2	NA	NA	NA
Rio Timbio	2.37	-76.71	1750	TERR	Legacy2	NA	NA	NA
Rockyhock Bay	36.17	-76.68	6	TERR	Legacy2	NA	NA	NA
Ruby Marsh	41.13	-115.51	1818	TERR	Legacy2	1	0	0
Rusaka Swamp	-3.43	29.62	2070	TERR	Legacy2	1	0	0
Sacred Lake	0.05	37.53	2345	TERR	Legacy2	3	2	2
Saint-Ursin	48.52	-0.25	234	TERR	Legacy2	3	0	0

San Agustin Plains (SAPBHM)	33.87	-108.25	2069	TERR	Legacy2	NA	NA	NA
Sangluoshu	37.50	117.73	50	TERR	Zhou et al. (2023)	NA	NA	NA
Sanshui K5	22.78	112.63	12	TERR	Zhou et al. (2023)	NA	NA	NA
Shaamar	50.20	105.20	650	TERR	Legacy2	2	0	0
Shuidonggou SDG2	38.28	106.50	1200	TERR	Zhou et al. (2023)	NA	NA	NA
Shunyi GZK1	40.15	116.53	50	TERR	Zhou et al. (2023)	NA	NA	NA
Siberia	-17.09	-64.72	2920	TERR	ACER	1	1	1
Siberia1	-17.09	-64.72	2920	TERR	Legacy2	1	1	1
Sihailongwan Maar Lake	42.28	126.60	797	TERR	Pangaea	8	1	1
Siluyanov Yar-2 Exposure	46.13	137.83	25	TERR	Legacy2	NA	NA	NA
Sirunki Wabag	-5.44	143.53	2550	TERR	Legacy2	2	0	0
St. Catherines Island (Northwest Marsh)	31.69	-81.15	0	TERR	Legacy2	NA	NA	NA
Stoneman Lake_STL	34.78	-111.52	2048	TERR	AUTHOR	3	0	0
Stracciacappa	42.13	12.32	220	TERR	ACER	4	0	0
Straldzha mire (QUARRY)	42.63	26.78	137	TERR	Legacy2	NA	NA	NA
Tagua Tagua - DIGI	-34.50	-71.16	200	TERR	ACER	6	1	1
Taiquemo	-42.17	-73.60	170	TERR	ACER	8	0	0
Tanon River	59.67	151.20	40	TERR	Cao et al. (2019, 2020)	NA	NA	NA
Tanon River [Quarry Site]	59.67	151.20	40	TERR	Legacy2	NA	NA	NA
Taymyr Lake SAO1	74.55	100.53	47	TERR	Cao et al. (2019, 2020)	NA	NA	NA
Tianshuihai TS95	35.35	79.52	4900	TERR	Zhou et al. (2023)	1	0	0
Tianyang Maar Lake TYC	20.52	110.30	108	TERR	Zhou et al. (2023)	3	0	0
Tianyang TY1	20.35	110.35	90	TERR	Zhou et al. (2023)	1	1	0
Tikhangou Exposure	42.83	132.78	4	TERR	Legacy2	NA	NA	NA
Toadlena Lake [Dead Man Lake] (DEAD5826)	36.24	-108.95	2759	TERR	Legacy2	1	0	0
Toadlena Lake [Dead Man Lake] (DEAD6101)	36.24	-108.95	2759	TERR	Legacy2	4	2	2
Tortoise Lagoon	-27.52	153.47	39	TERR	Legacy2	2	2	2
Toushe Basin	23.82	120.88	650	TERR	ACER	8	0	0
Toushe Lake 2013	23.82	120.88	650	TERR	Zhou et al. (2023)	1	0	0
Tswaing Crater	-25.40	28.08	1100	TERR	ACER	5	0	0

Tukuto Lake	68.50	-157.03	505	TERR	Legacy2	1	1	1
Tyrrendara Swamp	-38.20	141.76	13	TERR	ACER	NA	NA	NA
Ulan Buh Desert WL10ZK-1	40.04	105.78	1026	TERR	Zhou et al. (2023)	NA	NA	NA
Valle di Castiglione	41.90	12.76	44	TERR	ACER	7	3	3
Villarquemado	40.82	-1.48	985	TERR	AUTHOR	4	1	0
Vinillos	-0.60	-77.85	2090	TERR	Legacy2	1	0	0
Voordrag	-27.74	31.33	940	TERR	Legacy2	NA	NA	NA
W8709-13 PC	42.11	-125.75	-2712	MARI	ACER	NA	NA	NA
W8709-8 PC	42.26	-127.68	-3111	MARI	ACER	NA	NA	NA
Walker Lake	35.38	-111.71	2500	TERR	ACER	NA	NA	NA
Wenquangou	35.92	94.20	4700	TERR	Zhou et al. (2023)	NA	NA	NA
White Pond (WHITESC)	34.17	-80.78	90	TERR	Legacy2	NA	NA	NA
Wulagai Lake	45.42	117.48	822	TERR	AUTHOR	7	0	0
Xere Wapo	-22.30	166.96	235	TERR	Legacy2	NA	NA	NA
Xijir Ulan Lake	35.23	90.33	4500	TERR	Zhou et al. (2023)	NA	NA	NA
Xining ZK2	35.97	101.67	4363	TERR	Zhou et al. (2023)	NA	NA	NA
Yabulai Mt	39.62	103.92	1266	TERR	Zhou et al. (2023)	2	0	0
Yangerzhuang	38.35	117.35	5	TERR	Zhou et al. (2023)	NA	NA	NA
Yangjiapo	40.02	118.68	70	TERR	Zhou et al. (2023)	NA	NA	NA
Yangyuan-Caocun	40.10	114.40	875	TERR	Zhou et al. (2023)	1	0	0
Yaxi Co Lake	34.28	92.67	4000	TERR	Zhou et al. (2023)	NA	NA	NA
Zagoskin Lake	63.45	-162.11	7	TERR	Legacy2	5	0	0
Zhongshan PK19	21.80	113.30	6	TERR	Zhou et al. (2023)	NA	NA	NA

948

949

950 Table 2: Leave-out cross-validation (with geographically and climatically close sites removed)
 951 using fxTWA-PLSv2, for mean temperature of the coldest month (MTCO), mean temperature
 952 of the warmest month (MTWA) and plant-available moisture (α_{plant}). P-splines smoothed fx was
 953 estimated using 200 bins. n is the number of components used; Avg.bias is the average bias;
 954 RMSEP is the root-mean-square error of prediction; $\Delta\text{RMSEP}\%$ is the per cent change of
 955 RMSEP of the current number of components compared to using one component less, i.e. 100
 956 $\times (\text{RMSEP}_n - \text{RMSEP}_{n-1}) / \text{RMSEP}_{n-1}$. The p value assesses whether using the current number
 957 of components represents a significant ($p \leq 0.01$) difference over using one fewer component.
 958 To avoid over-fitting, the last significant number of components (i.e. the first insignificant
 959 number of components minus 1; p can become significant again after being insignificant with
 960 increasing n , but regarded meaningless) is selected for subsequent analyses and indicated in
 961 **bold**. The degree of overall compression is assessed by linear regression of the cross-validated
 962 reconstructions against the variable; b_1 and σ_{b_1} are the slope and the standard error of the slope,
 963 respectively. A slope (b_1) of 1 indicates no compression.

	n	R^2	Avg.bias	RMSEP	$\Delta\text{RMSEP}\%$	p	b_1	σ_{b_1}
MTCO ($^{\circ}\text{C}$)	1	0.72	-1.15	6.89	NA	NA	0.82	0.00
	2	0.73	-1.25	6.75	-2.00	0.001	0.83	0.00
	3	0.74	-1.20	6.66	-1.42	0.001	0.84	0.00
	4	0.74	-1.23	6.66	0.02	0.663	0.84	0.00
	5	0.74	-1.24	6.64	-0.31	0.001	0.84	0.00
	6	0.74	-1.24	6.63	-0.11	0.001	0.84	0.00
MTWA ($^{\circ}\text{C}$)	1	0.51	-0.32	4.00	NA	NA	0.64	0.00
	2	0.59	-0.22	3.67	-8.32	0.001	0.72	0.00
	3	0.60	-0.25	3.63	-0.95	0.001	0.72	0.00
	4	0.60	-0.25	3.62	-0.29	0.012	0.72	0.00
	5	0.60	-0.27	3.63	0.22	0.974	0.72	0.00
	6	0.60	-0.28	3.61	-0.61	0.001	0.72	0.00
α_{plant}	1	0.61	-0.020	0.191	NA	NA	0.65	0.00
	2	0.62	-0.022	0.190	-0.49	0.001	0.67	0.00
	3	0.63	-0.020	0.186	-2.07	0.001	0.68	0.00
	4	0.64	-0.020	0.186	-0.30	0.020	0.69	0.00
	5	0.64	-0.020	0.185	-0.18	0.003	0.70	0.00
	6	0.64	-0.020	0.185	0.09	0.988	0.70	0.00

964

965

966 Table 3: Maximum likelihood estimates of the relationship between the change in mean
 967 temperature of the coldest month (ΔMTCO) and the change in mean temperature of the
 968 warmest month (ΔMTWA) for the northern extratropics (NET, north of 23.5°N), tropics
 969 (TROP, between 23.5°N and 23.5°S) and southern extratropics (SET, south of 23.5°S). The
 970 intercepts were set to zero since both variables are changes.

Region		Coefficient	Standard error (SE)	Lower 95%	Upper 95%
NET	Slope	2.9	0.5	2.0	3.8
TROP	Slope	2.1	0.4	1.2	3.0
SET	Slope	1.5	0.7	0.2	2.8

971

972

973 Table 4: Maximum likelihood estimates of the relationship between the change in CO₂-
 974 corrected plant-available moisture ($\Delta\alpha_{\text{plant,corrected}}$) and the change in mean temperature of the
 975 warmest month (ΔMTWA) for the northern extratropics (NET, north of 23.5°N), tropics
 976 (TROP, between 23.5°N and 23.5°S) and southern extratropics (SET, south of 23.5°S). The
 977 intercepts were set to zero since both variables are changes.

Region		Coefficient	Standard error (SE)	Lower 95%	Upper 95%
NET	Slope	0.27	0.24	-0.21	0.74
TROP	Slope	0.02	0.01	0.01	0.04
SET	Slope	-0.03	0.02	-0.06	0.01

978

979

980 Table 5: Maximum likelihood estimates of the relationship between the change in mean
 981 temperature of the coldest month (ΔMTCO) and the change in mean temperature of the
 982 warmest month (ΔMTWA) over (ice-free) land in LOVECLIM simulations, for the northern
 983 extratropics (NET, north of 23.5°N), tropics (TROP, between 23.5°N and 23.5°S) and southern
 984 extratropics (SET, south of 23.5°S). The intercepts were set to zero since both variables are
 985 changes.

Region		Coefficient	Standard error (SE)	Lower 95%	Upper 95%
NET	Slope	1.15	0.02	1.11	1.2
TROP	Slope	1.34	0.05	1.25	1.44
SET	Slope	0.76	0.03	0.70	0.81

986

987